Pharmacological Regulation of Ischemia-Activated Pericyte Reprogramming and Differentiation for Post-Stroke Regeneration and Recovery

Margarita Lui

Thesis submitted to the University of Ottawa
in partial fulfillment of the requirements for the
MSc in Cellular and Molecular Medicine

Department of Cellular and Molecular Medicine
Faculty of Medicine
University of Ottawa

Abstract

Direct *in vivo* cellular reprogramming offers the potential for local neural replacement to promote post-stroke neural regeneration and recovery. Pericytes are perivascular cells involved in blood-brain barrier maintenance under physiological conditions but are reprogrammed into multipotent induced neural progenitor cells (i-NPCs) in response to ischemia. The atypical protein kinase C (aPKC)-CREB binding protein (CBP) pathway regulates ischemia-activated pericyte (a-pericyte) reprogramming and neuronal differentiation. Our previous work showed that the pathway inhibitor compound C (CpdC) facilitated a-pericyte reprogramming into i-NPCs in culture, and that monoacylglycerol lipase (Mgll) inhibitor JZL184 was able to promote NPC differentiation to generate newborn neurons by mimicking pathway activation. In this regard, we propose to use acute CpdC treatment followed by chronic JZL184 treatment to enhance reprogramming of a-pericytes into i-NPCs and subsequently promote their neuronal differentiation, ultimately improving post-stroke functional recovery. Using the endothelin-1 (ET-1)/L-NAME ischemic stroke model in a pericyte lineage tracing transgenic mouse line, I characterized the ability of a-pericytes in the ischemic lesion site to generate neural (i-NPC, newborn neurons) and non-neural (microglia and fibroblasts) cell types. The CpdC+JZL184 treatment had early effects on enhancing a-pericyte reprogramming efficiency to produce i-NPCs at 7 days post-stroke and promoting their differentiation to generate neuroblasts at 14 days post-stroke. However, it did not affect stroke volume and produced minimal alterations to the pattern of post-stroke motor function recovery. Interestingly, I discovered a novel role of tamoxifen treatment prior to stroke in regulating reprogramming of a-pericytes and efficacy of compound C treatment. These studies inform the necessity of optimization of drug delivery for better control over the timing and duration to directly target in vivo i-NPC reprogramming and reveal a novel pharmacological paradigm to control the aPKC-CBP pathway.

Table of Contents

List of Diagrams

List of Figures

List of Abbreviations

2-AG	2-arachidonoyl glycerol
ARA	arachidonic acid
αSMA	alpha smooth muscle actin
a-pericytes	ischemia-activated pericytes
AMPK	AMP-dependent kinase
aPKC	atypical protein kinase C
BSA	bovine serum albumin
CBP	CREB binding protein
CB1R	cannabinoid receptor 1
CB2R	cannabinoid receptor 2
COL1A1	collagen type 1
CpdC	compound C
DCX	doublecortin
ECs	endothelial cells
ESCs	embryonic stem cells
ET-1	endothelin-1
GFP	green fluorescent protein
HAT	histone acetyltransferase
i-neurons	induced neurons
i-NPCs	induced neural progenitor cells
I.P.	intraperitoneally
iPSCs	induced pluripotent stem cells
L-NAME	L-N^G-Nitroarginine methyl ester
MCAo	middle cerebral artery occlusion

Mgll	monoacylglycerol lipase
MSCs	mesenchymal stromal cells
NG2	neural glial antigen 2
NGS	normal goat serum
NPCs	neural progenitor cells
NSCs	neural stem cells
NVU	neurovascular unit
PBS	phosphate buffered saline
PBS-T	Triton X-100 in phosphate buffered saline
PFA	paraformaldehyde
PDGFRβ	platelet-derived growth factor receptor beta
SGZ	subgranular zone
SVZ	subventricular zone
TAM	tamoxifen
tPA	tissue plasminogen activator
VSMCs	vascular smooth muscle cells
YFP	yellow fluorescent protein

Acknowledgements

First and foremost, I would like to sincerely thank my supervisor, Dr. Jing Wang, for taking me on as your student. You have provided me with the opportunities to expand my skills and knowledge both in and out of the lab and have been a source of constant support and mentorship through the ups and downs of the last few years.

I'd like to extend my thanks to the members of the Wang Lab as well, especially Matthew Seegobin, Charvi Syal, Edward Sun, Allison Loan, and Dr. Joseph Leung, who have kindly offered their technical and emotional support throughout this journey. I also thank the amazing staff at ACVS and Behaviour Core without whom none of this work would be possible.

I would also like to thank my thesis advisory committee members, Dr. Diane Lagace and Dr. Simon Chen, for their valuable input during our meetings and their support and guidance in shaping my academic and professional development.

1.0 Introduction

1.1 Ischemic Stroke and its Impact

An ischemic stroke is caused by a blockage in cerebral blood flow, leading to the deprivation of oxygen and nutrients to the supplied tissue and eventually causing necrotic and apoptotic cell death in the affected area.[1,2] The cell death sets off excitotoxicity, oxidative stress, and inflammatory immune responses.[1,2] The stroke injury produces the classic stroke symptoms of face drooping, arm weakness, and slurred speech included in the F.A.S.T. warning signs, as well as a variety of other potential symptoms including sudden numbness, confusion, severe headache, vomiting, and trouble with vision or coordination. These symptoms are dependent on the extent and area of the brain that is impacted by ischemia.[2] The initial blockage can be caused by a locally derived thrombus or an embolus that travels through larger diameter vessels and gets lodged in a smaller vessel.[2] Once blood flow is cut off, the damage within the ischemic core, where blood flow is severely compromised, is irreversible. However, the tissues surrounding the core form an ischemic penumbra which is hypo-perfused but potentially rescuable due to the collateral blood flow that provides alternate routes for nutrient and oxygen supply.[3] The primary goal of stroke treatment is therefore to minimize the duration of ischemia to limit the severity of the injury.[2]

The only treatment that is currently approved for ischemic stroke is intravenous administration of tissue plasminogen activator (tPA).[1,2] However, its use is restricted to the first 3-4.5 hours following the onset of ischemia. After this time window, it may increase the risk of hemorrhage and greater complications and more invasive direct revascularization techniques are then needed.[1,2] Only a small percentage of stroke victims ever receive the tPA treatment and it is not always successful in many cases.[1,2] A majority of stroke victims survive but are left with disabilities such as loss of motor or sensory functions, chronic pain, problems producing or understanding language, cognitive impairments, and emotional disturbances.[4]

These can greatly reduce the quality of life for survivors. Although post-stroke rehabilitation is available, it requires that patients have a certain level of remaining ability and access to suitable resources and services.[5] It also depends highly on self-motivation to continue with the long-term treatment program.[5]

The combination of difficult treatment and recovery with a high incidence rate (1 in 4 individuals over a lifetime) has bolstered stroke as one of the leading causes of disability around the world and constitutes a significant financial burden on the healthcare system.[4] As both the general population ages and stroke prevalence increases in younger and healthier individuals who are traditionally considered to be at lower risk,[4] the urgent need to develop effective alternative therapeutic strategies for stroke recovery has become apparent over time.

1.2 Mouse Models of Ischemic Stroke

To gain a greater understanding of stroke processes and develop potential treatments, researchers have created several procedures to mimic ischemic stroke in rodents. Mouse ischemic stroke models are a particularly useful tool for their application in transgenic mouse lines to better understand the cellular and molecular basis of ischemic injury and repair. Ideally, a good animal stroke model replicates the relatively small infarct size, reperfusion of the injured area, and behavioural deficits followed by recovery of functions to a certain degree.[6] These 1features are typically exhibited in clinical cases of ischemic stroke. Currently, the most employed rodent stroke models are the middle cerebral artery occlusion (MCAo), photothrombosis, and endothelin-1 (ET-1) models.

The middle cerebral artery occlusion model involves suturing of the carotid artery to block blood flow to the middle cerebral artery, the most frequently impacted vessel in cases of human ischemic stroke.[7,8] The MCAo has also been modified to distal or embolic MCA occlusion procedures and the duration of occlusion can range from transient to permanent. This

model successfully recreates the ischemic core and penumbra with a relatively short surgery time, control over reperfusion timing, and no physical damage to brain tissue.[8] However, MCAo causes overly large infarcts that cover most of the targeted hemisphere, including the striatum, thalamus, subventricular zone, hippocampus, and cortex.[6,8] These sizes of stroke are typically malignant in humans and therefore reduce its clinical relevance.[6] MCAo also produces complications such as hypothermia.[6] Hypothermia regulates the ischemic injury itself,[9] making interpretation of stroke studies using this model more complex.

In the photothrombosis method, a light-sensitive dye, such as Rose Bengal, is injected and circulated through the body.[10] The dye is then activated by light at a stereotactically determined location to cause photo-oxidation. The photo-oxidation generates reactive oxygen species to damage local blood vessels and leads to the formation of thrombi that interrupt blood flow into the area.[10] This procedure creates small reproducible infarcts at a targeted functional subregion while being minimally invasive and requiring less surgical skill to accomplish.[10] Its primary drawback stems from its mode of injury. The photo-oxidation-induced vascular insult causes edema which is not observed in human stroke.[11,12] In addition, little to no penumbra region due to lack of collateral blood flow and reperfusion in the photothrombosis model limits the clinical translatability of this model.[6]

The endothelin-1 stroke model uses an intracerebral injection of the vasoconstrictive peptide ET-1 that acts on endothelin receptors on endothelial cells.[13,14] It can be administered in combination with the endothelial nitric oxide synthase inhibitor L-N^G-Nitroarginine methyl ester (L-NAME) to increase the potency of vasoconstriction.[13,14] Stereotactic injection of vasoconstrictive peptides not only allows for control over the location of ET-1 stroke but also allows targeting of diverse areas of the brain from superficial cortical regions to deeper subcortical regions.[13–15] The extent of the injury can be controlled by the dosage of ET-1. The ET-1 stroke exhibits the key characteristic of ischemia upon administration with gradual

reperfusion as the peptide breaks down over several hours.[16] Important limitations of the ET-1 model are the physical injury that is produced by the needle insertion and the activation of endothelial receptor-expressing neurons and astrocytes by ET-1 which promote axonal sprouting[17] and astrocyte proliferation[18] respectively. This complicates studies of innate neural repair involving these cells.

Together, these models of ischemia form the essential basis of animal stroke research. Since different stroke models feature their own strengths and weaknesses, every stroke study must begin with careful consideration of the characteristics of these experimental models that may affect the interpretation of results.

1.3 Neuroregenerative Strategies for Stroke Recovery

Following stroke, spontaneous recovery of function can occur. This has been attributed to neuroplasticity and neurogenesis.[19] Neuroplasticity refers to the reorganization of neural networks and is most closely associated with learning and memory, as well as adaptation and compensation in natural aging and neurological conditions.[20] In stroke, neuroplasticity is evident in changes to the activation of peri-infarct regions and attributed to molecular changes triggered by ischemia to induce axonal sprouting and synapse formation.[19,20] These are the processes that can be promoted by non-invasive stroke recovery strategies, such as task-based rehabilitation exercises and transcranial stimulation.[20] In comparison to these large-scale changes to connections between neurons, neurogenesis refers to the processes that give rise to new neurons from the pools of endogenous neural progenitor cells (NPCs) in the subventricular zone (SVZ) of the lateral ventricles and subgranular zone (SGZ) in the hippocampus. Following ischemia, adult NPCs in the SVZ are stimulated by ischemia, causing proliferation and differentiation into neuroblasts and migration towards the infarct region that is supported by an association with blood vessels.[21] However, most of these cells died off sooner after they

arrive at the injury site and cells that survive must then find across a barrier of glial scarring to integrate into local neural circuits.[22] Therefore, although many molecular pathways have been identified to regulate post-stroke neurogenesis, potential therapies to replace lost neurons are still in the early stages since many obstacles need to be overcome.

In addition to the promotion of neurogenesis from endogenous NPCs for stroke therapy, newer strategies have focused on cellular reprogramming, either through transplantation of exogenous reprogrammed NPCs or modulating direct *in vivo* cellular reprogramming. Cell transplantation involves the grafting of neural stem cells which can be derived from various sources, such as bone marrow, umbilical cord, and fetal brain tissues.[23] The development of induced pluripotent stem cells (iPSCs) that are reprogrammed from somatic cells, such as skin fibroblasts, in the last decade represented a revolutionary technology to produce autologous cells for transplantation.[24] Currently, a lot of effort has been made to study the effects of transplantation of human neural stem cells (NSC) derived from iPSCs on post-stroke regeneration and recovery in animal stroke models.[25] Once in place, the human iPSC-derived NSCs can differentiate into neurons as well as secrete factors that help to reduce inflammation and promote angiogenesis and endogenous neurogenesis in a phenomenon known as the bystander effect.[26,27] The major limiting factor for the use of this approach is that it requires direct access to the injured tissue, making it highly invasive and a less optimal approach for use in stroke patients.

In contrast to transplantation of reprogrammed NPCs made in the dish, *in vivo* cellular reprogramming directly converts non-neuronal cells into induced neural progenitor cells (i-NPCs) and induced neurons (i-neurons) *in situ. In vivo* cellular reprogramming is most commonly achieved through viral injections of key transcription factors involved in neuronal fate into the target brain region.[28–32] In particular, Sox2 expression alone reliably induces reprogramming whereas expression of other transcription factors, such as Ascl1, is not able to

drive this process on its own *in vivo*.[28,29] The generated i-neurons have been categorized into different neuronal subtypes and can become functionally integrated into local tissues, repairing damaged brain tissue and rescuing stroke.[30,32–36] Therefore, *in vivo* cellular reprogramming offers an ideal alternative to promoting endogenous neurogenesis and cell transplantation, providing a method for direct local neuronal replacement.

1.4 Pericytes and Ischemic Stroke

Pericytes are part of a group of contractile mural cells, along with vascular smooth muscle cells (VSMCs), that wrap around blood vessels and control vascular contraction and relaxation.[37,38] Pericytes are embedded in the basement membrane of microvessels such as arterioles, venules, and capillaries while VSMCs cover larger diameter arteries and veins.[38] Pericytes are morphologically diverse, taking the form of larger ensheathing pericytes or smaller mesh and thin-strand pericytes depending on their locations in the vascular system.[39] They are found throughout the body, including the heart, skeletal muscle, and brain.[38] However, the study of these cells is complicated by a lack of exclusive markers for pericytes, with most pericyte markers being expressed by multiple cell types. For example, neural glial antigen 2 (NG2) is expressed by both pericytes and oligodendrocyte precursors.[40–42] Alpha smooth muscle actin (αSMA),[43,44] vimentin,[44] and desmin[45] are found in pericytes as well as cells with contractile functions. Platelet-derived growth factor receptor beta (PDGFRβ)[46,47] and CD146[48,49] are more specifically associated with pericytes as they are important for pericyte recruitment and function at microvessels but are still found in other cell types. As a result, optimal identification of pericytes is based on a combination of morphology, localization, and expression of multiple markers.[37] A recently established marker, Tbx18, was shown to be selectively expressed by pericytes during development and throughout adulthood,[50] offering broader potential as a specific marker in pericyte studies.

Brain pericytes have been the subject of renewed interest in recent years due to their variety of functions within the neural environment. The main role of pericytes in the brain is to function as part of the neurovascular unit (NVU) that consists of vascular endothelial cells (ECs), pericytes, astrocytes, neurons, and basement membrane.[38,51] Proper function of the brain depends on proper blood flow through the nervous tissue to supply neurons and astrocytes with sufficient oxygen and nutrients to meet the high energetic demands on these cells.[38] Pericytes act as the bridge between the vascular and nervous systems, occupying a position between endothelial cells and neurons to control local cerebral blood flow in response to neuronal activity.[52] They are also directly involved in the proper development, function, and maintenance of vascular networks by regulating the cell cycle of ECs, releasing angiogenic factors, aiding in the formation of the basement membrane, and supporting healthy blood-brain barrier function.[53–56] Additionally, pericytes are sensitive to immune system signaling and facilitate immune cell entry into the brain.[57,58]

Perhaps the most unique trait of brain pericytes is their plasticity. Due to this feature, pericytes have often been compared to mesenchymal stromal cells (MSCs), a pool of adult stem cells found in several organs, including the brain, heart, liver, spleen, and bone marrow, which typically give rise to osteoblasts, adipocytes, and chondrocytes *in situ*.[59,60] Asides from their widespread presence throughout the body, the two cell types also share a developmental origin from the neural crest and localization beside blood vessels.[61] The exact distinction between pericytes and MSCs is debatable due to these commonalities but MSCs are typically identified by a different set of markers from pericytes[62] and pericytes are distinct in their vascular roles of angiogenic regulation and support.[63,64] MSCs and brain pericytes can both give rise to a variety of cell types, including mesenchymal cells (osteoblasts, adipocytes, and chondrocytes),[65,66] endothelial cells,[65,67] and fibroblasts.[68–70] However, brain pericytes stand

apart from MSCs in their greater propensity toward differentiation into CNS-specific cells like microglia[66,71] and neural lineage cells.[66,72–74]

Specifically, pericytes in the brain are readily reprogrammed into induced neural progenitor cells in response to ischemia. A study by Nakagomi *et al.* (2009) first described a substantial group of locally derived cells expressing Nestin, Nanog, Pax6, and Sox2, markers of neural progenitor cells, exclusively in the ischemic core in the cortex of adult mice 7 days after a permanent MCAo procedure. These cells, when isolated and cultured, formed neurosphere-like clusters that later generated electrically active neurons.[75] In a follow-up study, they observed that between 1 and 3 days after ischemia, these i-NPCs expressed PDGFRβ and increasingly populated the pia mater, migrating into layer I of the cortex along local vasculature with close association with CD31+ endothelial cells of blood vessels.[76] By 7 days post-stroke, the i-NPC population was significantly decreased.[76] They also co-expressed Sox10, a marker for neural crest cells, implying that these i-NPCs are derived from brain pericytes.[76] Additionally, expression of doublecortin (DCX), a neuroblast/immature neuron marker, in the i-NPCs by day 3 post-stroke was found, providing evidence for the beginnings of i-NPC differentiation occurring *in vivo.* Subsequent research by other groups, including us, has produced similar findings that i-NPCs derived from ischemia-activated pericytes (a-pericytes) are capable of differentiation in the ischemic core in both transient MCAo and ET-1 stroke models that mimic clinically relevant conditions of ischemia with reperfusion.[66,77,78] Evidence of these i-NPCs is highly valuable as they show neurogenic potential in the area of tissue that suffers the greatest degree of cell loss due to ischemic injury. Further, ischemia-activated pericytes can form microvessels that provide nutrient support to i-NPCs and their progeny to enhance cell survival and regeneration of lost tissue at the lesion site.[79] With the recent identification of pericyte-derived i-NPCs in the ischemic core following stroke in humans,[65]

pericytes increasingly appear to be ideal candidates in the development of therapeutic strategies in neural regeneration.

1.5 The aPKC-CPB Pathway in Reprogramming and Differentiation

Epigenetic regulation has increasingly been discovered to be involved in several neurological conditions, including stroke.[80,81] Studies have also uncovered the particular importance of epigenetic mechanisms for controlling both neuronal differentiation and cellular reprogramming,[82,83] setting them up to be promising targets in regenerative therapies. The aPKC-CBP pathway is one such mechanism that has been characterized to impact both neuronal differentiation and NPC reprogramming.

The role of aPKC (atypical protein kinase C)-CBP (CREB binding protein) pathway in neurogenesis was first explored when it was discovered that loss of CBP impairs the differentiation of cortical NPCs during brain development in a mouse model of Rubinstein-Taybi syndrome, a neurodevelopmental disorder associated with the deletion or mutation of one allele of CBP.[84] CBP is a transcriptional coactivator that promotes neurogenesis through its function as a histone acetyltransferase (HAT) at the promoters for neuronal differentiation genes.[84] Further investigation revealed that the neurogenic actions of CBP depended on aPKC-mediated phosphorylation at its serine (S) 436 site.[84] AMP-dependent kinase (AMPK) was then identified as an upstream regulator of the aPKC-CBP pathway in NPCs,[85] establishing a cascade of molecular events where AMPK activates aPKC to phosphorylate CBP and trigger neuronal differentiation. Activation of the aPKC-CBP pathway via AMPK activation has been shown to promote NPC differentiation and improve functional recovery following hypoxia/ischemia in neonatal mouse pups, showing great therapeutic potential.[86]

Conversely, the lack of a functional aPKC-CBP pathway causes a deficit in neurogenesis with the accumulation of NPCs in the brain. In aged mice possessing a *Cbp*S436A

phosphomutant that lacks the aPKC-mediated CBP phosphorylation site due to a replacement of serine with alanine (A), the population of NPCs in the hippocampus was significantly increased compared to wildtype mice.[87,88] Interestingly, this CBP phosphomutant mouse line also exhibits greater reprogramming of ischemia-activated pericytes into i-NPCs following stroke.[78] Unpublished work from our lab has investigated the mechanisms underlying this reprogramming facilitated by aPKC-CBP inhibition. CBP is known to acetylate Sox2,[89,90] a key transcription factor for stemness and NPC fate[91] and powerful reprogramming agent,[29,92] and facilitate its nuclear export and degradation.[89] We found that this phosphomutant CBP resulted in decreased Sox2 acetylation and increased Sox2 nuclearization, enhancing the production of NPCs. Altogether, this dynamic function of the aPKC-CBP pathway presents a signaling-directed epigenetic pathway featuring multiple molecules that can be potentially targeted to induce reprogramming of a-pericytes into i-NPCs via inhibition of the pathway while promoting neuronal differentiation via activation of the pathway.

1.6 Pharmacological Regulators of the aPKC-CBP Pathway

1.6.1 Compound C

Compound C (CpdC) is a pharmacological inhibitor of AMPK that is commonly used across many disciplines, from basic research to clinical applications. Within the body of stroke research, it has been investigated for its neuroprotective properties due to AMPK's function as a critical energy sensor in the cell, responding to ischemia by rapidly upregulating its activity to increase metabolic processes and gene expression.[93] Studies have shown that treatment with compound C (10 mg/kg) between onset and up to 2 hours following a 2-hour transient MCAo procedure in mice resulted in decreased stroke volume and improved scores on neurological function measured 24[94,95] and 72 hours[95] later following stroke. These beneficial effects following compound C treatment are associated with a transient decrease in AMPK

phosphorylation (reflective of decreased AMPK activity) at 4 hours post-stroke compared to control stroke mice.[94] In addition, the beneficial effects were time-dependent, losing efficacy with more delayed compound C administration.[95] Similarly, in Sprague Dawley rats that underwent a 60-minute MCAo procedure, treatment with compound C 1 hour after stroke reduced infarct size and neurological deficits measured at 24 hours post-stroke. In contrast, treatment with an AMPK activator, AICAR, significantly exacerbated ischemic injury,[95,96] highlighting the role of early AMPK activation in determining stroke outcomes.

Since inactivation of the aPKC-CBP pathway facilitated i-NPC reprogramming following stroke,[78] our group asked whether inhibition of its upstream signalling molecule, AMPK, using compound C could produce the same reprogramming effect. Treatment with compound C *in vitro* successfully enhanced the production of i-NPCs from ischemia-activated pericyte in comparison to control DMSO treatment, similar to the enhanced i-NPC reprogramming observed in *Cpb*S436A mice.[78] Additional unpublished work showed that this increased i-NPC reprogramming in compound C treated a-pericytes was likewise associated with decreased Sox2 acetylation and increased Sox2 nuclearization. Thus, it is important to evaluate whether compound C treatment *in vivo* following ischemia confers the same enhancement in a-pericyte to i-NPC reprogramming, which will help in understanding this novel role of compound C as a post-stroke therapy.

1.6.2 JZL184

JZL184 is a selective inhibitor of monoacylglycerol lipase (Mgll) that interacts directly with the enzyme via irreversible covalent bonds.[97] Mgll is the primary hydrolyzer of the endogenous endocannabinoid 2-arachidonoyl glycerol (2-AG), producing arachidonic acid (ARA).[98] Mgll inhibitors have been considered powerful potential therapeutic agents since 2-AG is involved in several key biological processes, including metabolism, neurogenesis,

inflammation, and analgesia, through cannabinoid receptor 1 (CB1R) and 2 (CB2R) signaling.[99] JZL184 has recently been investigated as a treatment for ischemic stroke due to its ability to block 2-AG hydrolysis, preventing the generation of ARA, a precursor in the biosynthesis of inflammatory compounds, such as prostaglandins.[99,100] A single treatment with JZL184 administered intraperitoneally across a range of dosages (4, 8, and 16 mg/kg JZL184) immediately following permanent MCAo in mice decreased brain infarct size, edema, and severity of functional deficits at 48 hours post-stroke compared to non-treated mice who underwent the same stroke procedure.[101] These effects were accompanied by lower levels of inflammation and oxidative stress.[101] In an experiment with adult spontaneously hypertensive rats and normal Wistar Kyoto rats using transient MCAo and ET-1 stroke models, intraperitoneal (I.P.) treatment with JZL184 one hour following stroke induction produced similar reductions in stroke volume and neuroinflammatory markers by 24 hours post-stroke and better improvements in functional recovery up to 28 days post-stroke compared to untreated animals.[99]

In our lab, JZL184 has been shown to promote neuronal differentiation by inhibiting the activity of Mgll whose expression is repressed by activation of the aPKC-CBP pathway. In *Cbp*S436A mice where the aPKC-CBP pathway is defective, deficits in hippocampal neurogenesis and hippocampal-dependent memory are associated with increased hippocampal Mgll expression. Interestingly, daily I.P administration with JZL184 at 8 mg/kg restored impaired neuronal differentiation and spatial memory to levels comparable to wild-type mice.[88] It was then determined that in addition to promoting neural gene expression, activation of the aPKC-CBP pathway enhances neuronal differential of NPCs through the repression of Mgll expression, increasing 2-AG-CB2R signalling to facilitate neuronal differentiation.[88] Therefore, Mgll inhibition presents a new therapeutic approach for promoting post-stroke neurogenesis by inducing NPC differentiation.

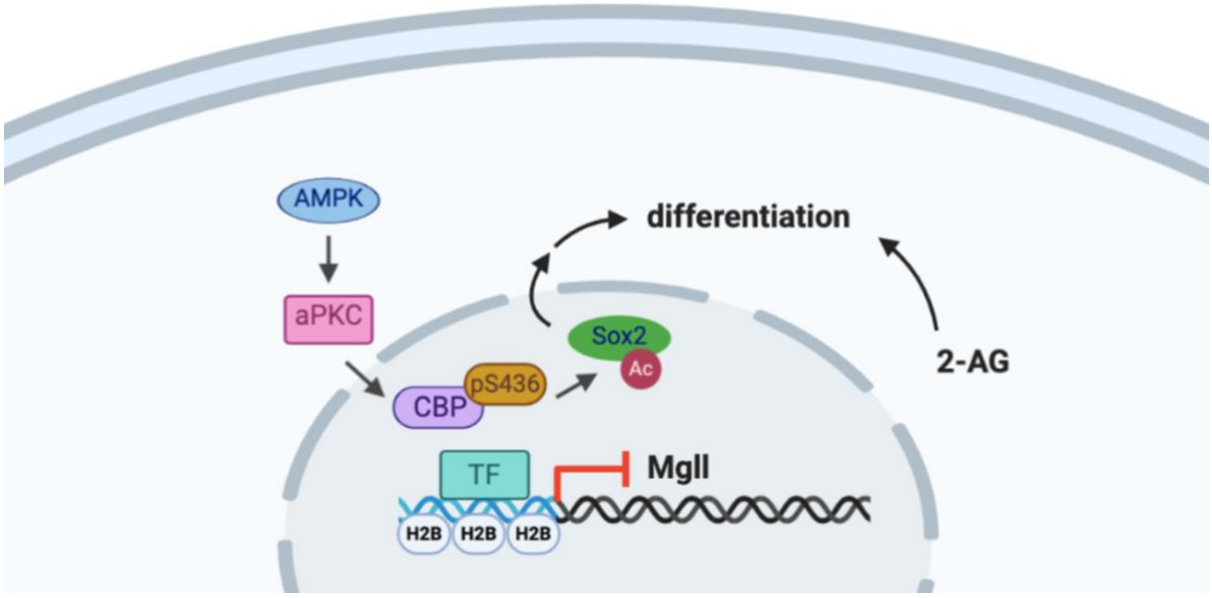

Diagram 1: AMPK-mediated activation of the aPKC-CBP pathway causes phosphorylation of CBP at S436 to promote neuronal differentiation by inhibiting Mgll-mediated hydrolysis of 2-AG and acetylating Sox2.

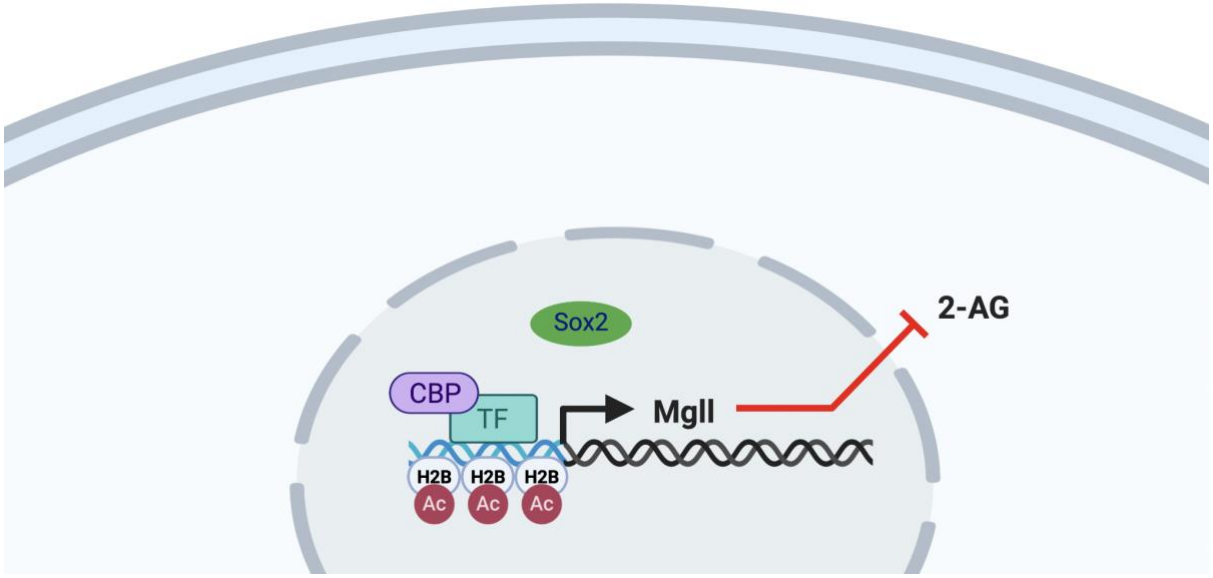

Diagram 2: Inhibition of the aPKC-CBP pathway promotes Mgll-mediated hydrolysis of 2-AG and Sox2 nuclearization for NPC maintenance.

1.6.3 Combination Treatment for Reprogramming and Differentiation

Compound C and JZL184 have been demonstrated to confer neuroprotection when administered immediately after ischemia, manifesting its effects in the acute phase of post-stroke. However, they both have been shown to mediate aPKC-CBP pathway activity, where compound C enhances reprogramming of a-pericytes into i-NPCs by inhibiting the pathway and JZL184 enhances neuronal differentiation in a manner analogous to the pathway activation. In this regard, I propose to determine whether sequential treatment with compound C followed by JZL184 can facilitate the production of i-neurons from a-pericytes via the i-NPC stage.

Hypothesis and Objectives

2.1 Hypothesis

Initial transient inactivation of the aPKC-CBP pathway by compound C followed by chronic treatment with JZL184 to mimic pathway activation will increase a-pericyte reprogramming into i-NPCs and subsequent i-NPC differentiation into i-neurons, ultimately promoting local neural regeneration and functional recovery. To test the hypothesis, I conducted the following three objective studies:

2.2 Objectives

Objective 1: Lineage trace a-pericyte reprogramming potential following ischemic stroke.

Objective 2: Evaluate the effect of combination drug treatment targeting the aPKC-CBP pathway on a-pericyte reprogramming and differentiation following ischemic stroke.

Objective 3: Assess the effects of the combination drug treatment on stroke volume and motor function recovery following ischemic stroke.

3.0 Materials and Methods

3.1 Animal Care and Housing

All animal use was approved by the Animal Care Committees of the University of Ottawa in accordance with the Canadian Council of Animal Care policies. The conditional transgenic mouse line Tbx18-CreERT2/YFP-flx was used to enable the timed labelling of Tbx18+ pericytes with yellow fluorescent protein for lineage tracing through the post-stroke period. The mice were maintained on a 12-hour light, 12-hour dark cycle with *ad libitum* access to food and water. Heterozygous Tbx18-CreERT2 (purchased from JAX, strain #031520) mice were crossed with homozygous YFP-flx mice (a gift from Dr. Diane Lagace) to produce offspring for the experiments. Only offspring that were heterozygous for both genes were used.

3.2 Tamoxifen Treatment

Animals (2-3 months) were treated with tamoxifen (TAM) to induce genetic recombination and enable YFP expression in Tbx18+ cells specifically. Tamoxifen solution was prepared at a concentration of 30 mg/mL (Sigma-Aldrich, T5648) in a solution of 10% anhydrous ethyl alcohol and 90% sunflower seed oil (Sigma-Aldrich, S5007). The solution was vortexed and then sonicated in a 4°C water bath for 15 minutes before use.

Mice initially received I.P. injections of tamoxifen at a dosage of 160 mg/kg daily for 5 days. Due to the increased mortality of these animals during treatment, the dosage was subsequently reduced to 120 mg/kg daily for 4 days for later cohorts. A one-week washout period was allowed before the animals underwent the ET-1/L-NAME surgery.

3.3 ET-1/L-NAME Preparation and Stereotaxic Surgery

To prepare the ET-1/L-NAME solution, L-NAME (Sigma-Aldrich, N5751) was first dissolved in sterile 1X phosphate-buffered saline (PBS) at 2.7 μg/μL. ET-1 (Abcam,

AB120471) was then dissolved in the L-NAME solution at 2.0 μg/μL. The ET-1/L-NAME solution was sonicated in a 4°C water bath for 15 minutes and kept on ice during the surgery.

Mice were anesthetized using 4% isoflurane and 1.5% oxygen in an induction chamber and maintained at 1-2% isoflurane and 1.5% oxygen when mounted to the stereotaxic frame. Surgical preparation included administration of 1 mL of warmed saline subcutaneously, xylocaine gel into each ear canal, and ophthalmic gel to each eye. Body temperature was monitored and maintained at 37°C throughout surgery using a rectal thermometer and heating pad. Intracranial injections of ET-1/L-NAME were performed using a 10 uL gastight glass syringe (Hamilton, 7653-01) with a 26G cemented needle (Hamilton, 80366) at the following two coordinates targeting the sensorimotor cortex: +0.0 mm anterior-posterior (AP), +2.0 mm medial-lateral (ML), -1.6 mm dorsal-ventral (DV); +0.2 mm AP, +2.0 mm ML, -1.4 mm DV. One bur hole was opened at the first coordinate using a microdrill to accommodate both injections. A one-minute-long delay before injection upon insertion of the needle was allowed for the tissue to settle. The solution was injected at a rate of 0.2 μL per minute with a target volume of 1 μL, containing 2.0 μg ET-1 and 2.7 μg L-NAME per injection site. A three-minute-long delay following injection was allowed to reduce backflow upon withdrawal of the needle. Bupivacaine was applied to the sealed incision site and 0.1 mL of buprenorphine was administered subcutaneously immediately following surgery. Buprenorphine was administered again at 4-hours post-operation as required. The approximate surgery time per mouse was 30 minutes.

3.4 Compound C and JZL184 Drug Treatments

Compound C (dorsomorphin dihydrochloride) (Abcam, 144821) was prepared in sterile 1X PBS at a concentration of 1 mg/mL. JZL184 (Cayman Chemical Compound, 13158-5) was prepared in DMSO at 40 mg/mL, then mixed with 2.5% Tween™ 80 in sterile 1X PBS to 0.8

mg/mL. 24 hours following the ET-1/L-NAME surgery, mice received I.P. injections of either compound C (10 mg/kg) or vehicle 1X PBS daily for 5 days. A two-day washout period occurred before mice that were treated with compound C received I.P. injections of JZL184 (8 mg/kg) every two days for 4 weeks. Likewise, mice that had been treated with sterile 1X PBS continued to receive I.P. injections of vehicle solution (2% DMSO, 2.5% Tween™ 80 in sterile 1X PBS) every two days for 4 weeks.

3.5 Tissue Preparation

At 3, 7, 14 or 35 days post-surgery, mice were anesthetized with 0.1 mL of sodium pentobarbital (65 mg/mL, I.P.). The animals were transcardially perfused with 35 mL of ice-cold 1X PBS (7 mL/minute for 5 minutes), followed by 35 mL of ice-cold 4% paraformaldehyde (PFA) (Sigma-Aldrich, 158127) in 1X PBS. The brains were dissected out and transferred to 4% PFA overnight at 4°C, then dehydrated in 30% sucrose solution with 0.1% sodium azide (Fisher, 19038-1000) for 2 days at 4°C. Samples were embedded in optimal cutting temperature compound (VWR, 95057-838) in a plastic molding tray (Fisher, 22-363-554) and flash-frozen on dry ice. Serial 20 µm-thick sections of the ischemic lesion were obtained using a cryostat (Leica Biosystems, CM1850) and sequentially collected on 10 Superfrost™ Plus glass microscope slides (Fisher, 12-550-15). Slides were stored at -80°C until needed.

3.6 Immunohistochemistry

Frozen sections were defrosted at 37°C for 10 minutes and washed three times with 1X PBS for 5 minutes each. The sections were blocked and permeabilized using 10% normal goat serum (NGS) (Invitrogen, Thermo Fisher Scientific, 10000C) if using non-goat primary antibodies, or 3% bovine serum albumin (BSA) (New England BioLabs, 9998S) if using a goat

primary antibody, in a 0.3% Triton™ X-100 (Fisher, BP151-100) in 1X PBS solution (PBS-T) for at least one hour at room temperature. Primary antibodies were incubated overnight at 4°C in their respective blocking/permeabilizing solutions. The antibodies used were chicken anti-GFP (1:1000) (Abcam, ab13970), rabbit anti-Sox2 (1:200) (Millipore, AB5603MI), goat anti-DCX (1:200) (Santa Crus, sc-8066), guinea pig anti-NeuN (1:1000) (Millipore, ABN90), rat anti-CD31 (1:200) (BD Biosciences, 550274), rabbit anti-COL1A1 (1:500) (OriGene Technologies, R1038), rabbit anti-Iba1 (1:1000) (Wake Chemicals, 019-19741).

Following the primary antibody incubation, the sections were washed three times with 1X PBS for 5 minutes each and incubated for one hour at room temperature with the following Alexa Fluor-conjugated secondary antibodies in 0.3% PBS-T at a 1:500 concentration: goat anti-chicken Alexa Fluor 488 (Invitrogen, Thermo Fisher Scientific, A-11039), donkey anti-rabbit Alexa Fluor 647 (Invitrogen, Thermo Fisher Scientific, A21206), donkey anti-goat Alexa Fluor 555 (Invitrogen, Thermo Fisher Scientific, A-21432), goat anti-guinea pig Alexa Fluor 647 (Invitrogen, Thermo Fisher Scientific, A21450), goat anti-rat Alexa Fluor 555 (Invitrogen, Thermo Fisher Scientific, A-21434), donkey anti-rabbit Alexa Fluor 555 (Invitrogen, Thermo Fisher Scientific, A-31572). After secondary antibody incubation, sections were counterstained with Hoechst 33342 (Cell Signaling Technology, 4082) at 1:1000 in 0.3% PBS-T for 5 minutes and then washed three times with 1X PBS for 5 minutes each. Slides were mounted with glass coverslips using PermaFluor™ mounting medium (Thermo Fisher Scientific, TA-030-FM) and dried overnight at room temperature.

3.7. Imaging and Quantification

Fluorescent images were taken on a Zeiss Imager M1 fluorescent microscope with Zeiss Axiovision software, a Zeiss Image M2 fluorescent microscope with Zeiss Zen Blue software, or a Zeiss LSM 800 confocal microscope using Zeiss Zen Pro software, all containing z-axis

capability. Images were captured at 20X magnification with the z-axis per section set at 1 μm apart and processed as an optical stack of 10-15 scanned slices for quantification. Images were taken from left to right of the infarct region, adhering to the pia surface border to maintain comparable areas of quantification within the lesion between animals. One to five images per section were taken for two to nine sections of a sample, depending on the time point post-stroke and the extent of ischemic damage. The total number of YFP+ cells and the number of YFP+ cells that co-expressed another cell type marker were quantified in FIJI software.

3.8 Ladder Rung Test

Mice were placed at one end of a horizontal ladder made of plexiglass walls with irregularly placed metal rungs set on top of two cages. The home cage was placed at the opposite end of the ladder. The animals were videotaped crossing the ladder with footage shot from slightly below so that all four limbs are visible for analysis. Mice underwent one day of training and one day of pre-surgery baseline performance measurement, then retested at 7, 14, and 35 days post-surgery. Between each testing time point, the orientation of the ladder and cages was flipped so the mouse would have to traverse the ladder starting from the opposite side of the room to minimize improvement from learning memory. A maximum of five trials per day were filmed for each mouse and the three best trials (no interruptions in movement across ladder) were scored for the total number of steps and the total number of errors made in each limb. An error was considered as a miss, a slip, or a cheat (use of the wall to support weight). The trial footage was analyzed in VLC media player at 0.06x speed. The difference in percentage error for each limb from baseline performance at each time point was calculated as:

$$\text{difference in \% error from baseline} = \left(\frac{\text{total misses + slips + cheats}}{\text{total limb steps}}\right)*100\% - \left(\frac{\text{baseline total misses + slips + cheats}}{\text{baseline total limb steps}}\right)*100\%$$

3.9 Cylinder Test

Mice were placed in a clear cylinder container under moderate lighting and videotaped from above for the duration of 20 rears. A pre-surgery baseline performance measurement was taken and mice were retested at 7, 14, and 35 days post-surgery. The videos were analyzed in VLC media player at 0.06x speed and the number of ipsilateral, contralateral, and both paw touches to the cylinder wall was counted. The percentage ipsilateral preference at each time point was calculated as:

$$\%\ \text{ipsilateral preference} = \left(\frac{\text{total ipsilateral paw touches - total contralateral paw touches}}{\text{total ipsilateral, contralateral, and both paw touches}}\right) * 100\%$$

3.10 Grid Walk Test

Mice were placed on an approximately 1 ft. x 1 ft. square metal grid with 1 cm spacing that was elevated 1 ft. above the surface of a table and videotaped from below for three minutes while the animals roamed freely. A pre-surgery baseline performance measurement was taken and mice were retested at 7, 14, and 35 days post-surgery. The total number of steps in each forelimb and the number of errors in the form of slips and misses made by each forelimb were counted in VLC media player at 0.06x speed. The percentage error for each forelimb at each time point was calculated as:

$$\%\ \text{steps with error} = \left(\frac{\text{total forelimb slips + misses}}{\text{total forelimb steps}}\right) * 100\%$$

3.11 Cresyl Violet Staining

Frozen sections were defrosted at 37°C for 10 minutes. The slides were loaded into a vertical slide staining rack and immersed in cresyl violet working solution consisting of 0.2% cresyl violet (Sigma-Aldrich, C5042) dissolved in 0.5% acetic acid buffer solution, pH 3.5, for 30 minutes. The racked slides were then sequentially dehydrated in 70%, 95%, and 100% anhydrous ethyl alcohol and cleared in CitriSolv™ (Fisher, 04-355-121). Slides were mounted

with glass coverslips using Permount™ mounting medium (Fisher, SP15-100) solution and dried overnight at room temperature.

3.12 Infarct Volume Measurement

Brightfield images of cresyl violet-stained whole tissue sections were captured using a Zeiss AxioScan slide scanner at 10X magnification. Images were analyzed using QuPath software. The infarct area was measured on every section on the slide and edema-adjusted infarct volume in mm^3 was calculated using the following equation:

$$E_A\text{-infarct volume in } mm^3 =$$

$$\sum\left(\text{infarct area in mm}\left(\frac{\text{contralateral hemisphere area in mm}}{\text{ipsilateral hemisphere area in mm}}\right)\right) * 0.02 \text{ (section thickness in mm)} * 10 \text{ (serial collection factor)}$$

3.13 Statistical Analysis

All data analysis was conducted using GraphPad Prism 9 software. Statistical analyses were performed using a two-tailed student t-test or one-way or two-way ANOVA with Tukey's post hoc test. All values are expressed as mean ± standard error of the mean. All comparisons were analyzed using $\alpha = 0.05$.

4.0 Results

4.1 Pericytes are reprogrammed into neural and non-neural cell types following ischemic stroke.

To lineage trace pericytes before stroke, Tbx18-Cre-ERT2/YFP-flx mice were treated with tamoxifen at a dosage of 160 mg/kg daily for 5 days, followed by a one-week washout period before ET-1/L-NAME surgery. Characterization of cell identities of Tbx18-YFP+ pericytes following stroke was performed at 3, 7, and 14 days post-stroke (Figure 1A, B). At 3 days post-stroke, 85.19% of total Tbx18-YFP+ cells were adjacent to CD31+ blood vessels. This association decreased over time across the 7 day (67.44%) and 14 day (61.22%) time points, suggesting a gradual loss in their typical perivascular support function (Figure 1C). On the other hand, the Tbx18-YFP+ cells expressed markers of both neural and non-neural cell types following stroke injury. Collagen type 1 (COL1A1), a marker for fibroblasts, was co-expressed in a consistent proportion of Tbx18-YFP+ cells, making up 28.04% of YFP+ cells at 3 days, 22.72% at 7 days, and 27.45% at 14 days post-stroke (Figure 1D). Iba1, a marker for microglia, had its highest expression in Tbx18-YFP+ cells early on at 3 days post-stroke, making up 24.66% of YFP+ cells, and decreased in the later tested time points (13.11% at 7 days and 9.26 at 14 days) (Figure 1E).

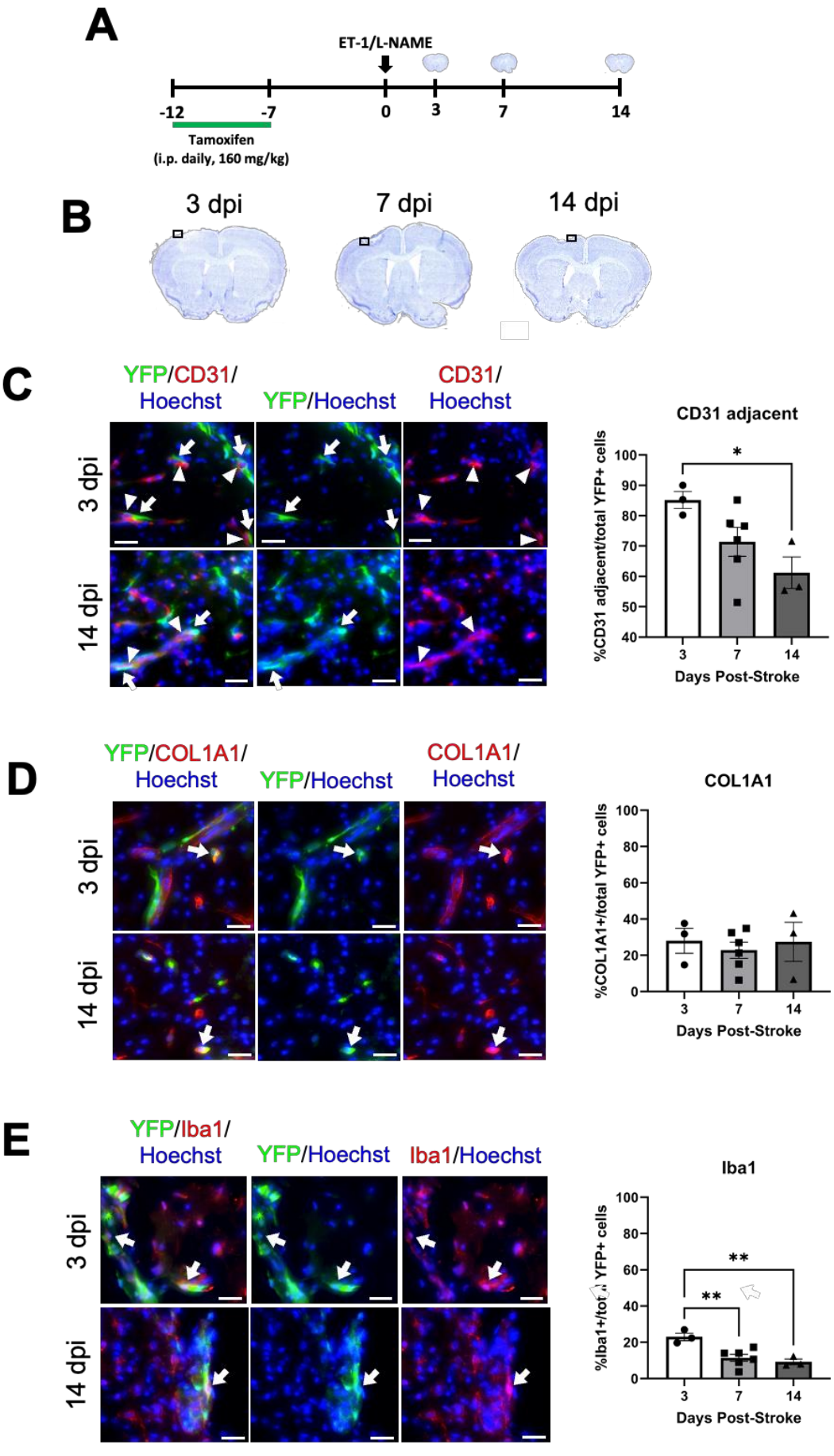
A
ET-1/L-NAME
-12
-7
0
3
7
14
Tamoxifen
(i.p. daily, 160 mg/kg)
B
3 dpi
7 dpi
14 dpi
C
YFP/CD31/
Hoechst
YFP/Hoechst
CD31/
Hoechst
3 dpi
14 dpi
CD31 adjacent
%CD31 adjacent/total YFP+ cells
Days Post-Stroke
D
YFP/COL1A1/
Hoechst
YFP/Hoechst
COL1A1/
Hoechst
COL1A1
%COL1A1+/total YFP+ cells
Days Post-Stroke
E
YFP/Iba1/
Hoechst
YFP/Hoechst
Iba1/Hoechst
Iba1
Days Post-Stroke

Figure 1: Ischemia-activated pericytes in the stroke lesion are reprogrammed into fibroblasts and microglia, reducing vascular association over time. (A) Experimental timeline of TAM pre-treatment, ET-1/L-NAME surgery, and tissue collection for analysis at 3, 7, and 14 days post-stroke. **(B)** Cresyl violet image of representative area for identification of cells in the stroke lesion at 3, 7, and 14 days post-stroke. **(C-E)** Quantification and images of the proportion of Tbx18-YFP+ (green) cells that were **(C)** CD31 adjacent, **(D)** COL1A1+, and **(E)** Iba1+ (red) at 3, 7, and 14 days post-stroke. Arrows denote co-labelled cells, arrowheads in (A) denote adjacent CD31+ cells. Scale bars = 20 μm. Data analyzed by one way ANOVA ($F_{2,9} = 4.381$, $p = 0.0469$ for CD31, $F_{2,9} = 4.2078$, $p = 0.8162$ for COL1A1, $F_{2,9} = 10.16$, $p = 0.0049$ for Iba1) with Tukey's post-hoc test between time points (n=3-6 animals per time point, * $p < 0.05$, ** $p < 0.01$).

Approximately half of the Tbx18-YFP+ cells stably expressed the pluripotency and NPC marker, Sox2, in either the cytoplasm or nucleus across all time points (46.08% at 3 days, 48.41% at 7 days, and 48.24% at 14 days post-stroke) (Figure 2A, B). To examine the population of ischemia-activated pericytes that have been fully reprogrammed into i-NPCs in the stroke lesion, the proportion of nuclearized Sox2 fluorescent signal in the Sox2+/YFP+ cells was quantified. The highest proportion of nuclearized Sox2 was at 3-day post-stroke, making up 6.09% of this subpopulation. This proportion decreased over time to 3.19% at 7 days and 0.35% at 14 days (Figure 2C). The neuroblast marker, DCX, was modestly expressed in Tbx18-YFP+ cells at 3 and 7 days post-stroke (5.94% and 4.75% respectively) and was greatly increased at day 14 following stroke injury (12.67% of YFP+ cells) (Figure 3A). Lastly, the mature neuron marker, NeuN, was only found in Tbx18-YFP+ cells on day 14 after stroke injury, representing 3.32% of the total Tbx18-YFP+ population (Figure 3B).

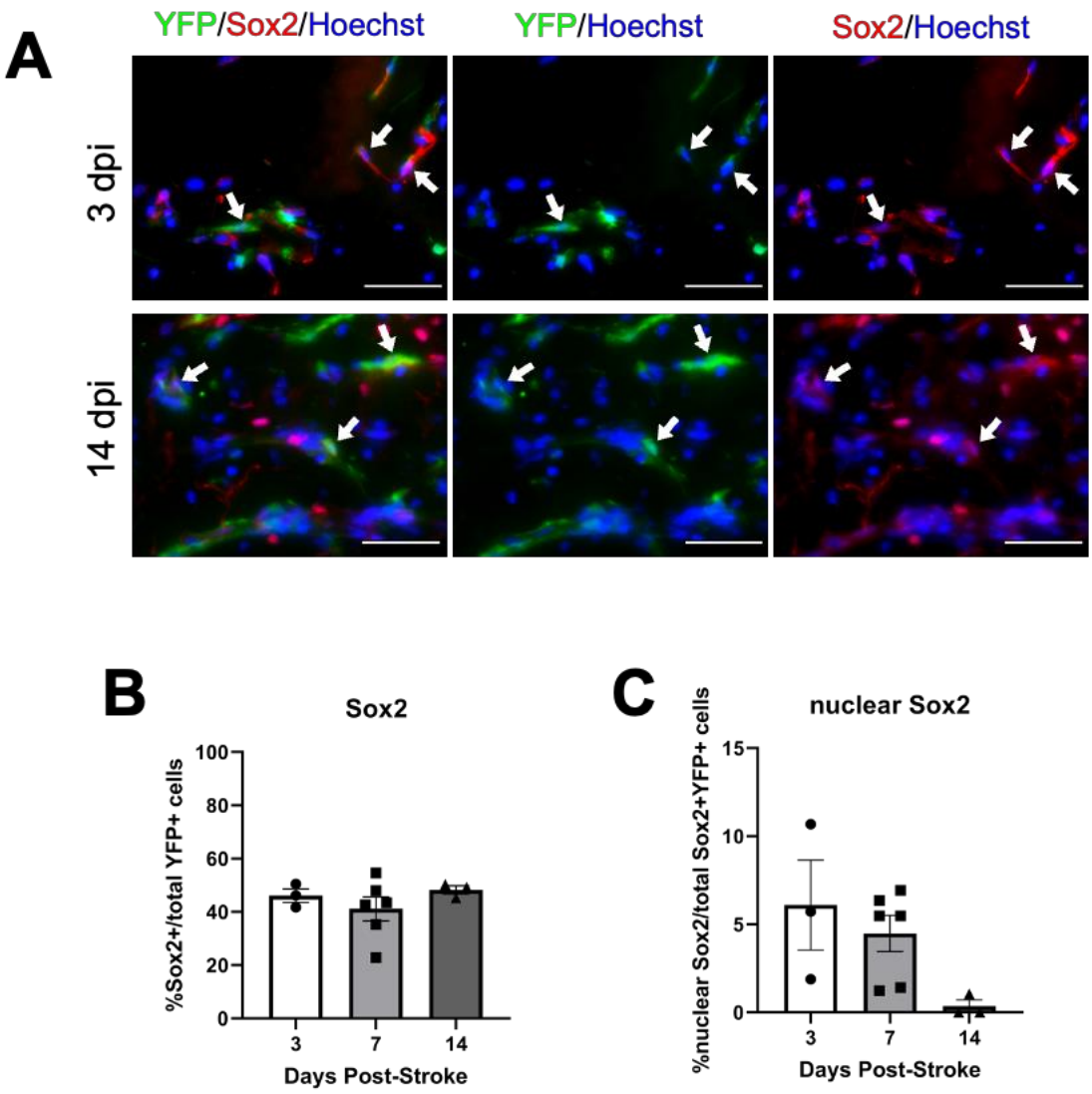

Figure 2: Ischemia-activated pericytes in the stroke lesion are reprogrammed into multipotent i-NPCs. (A-C) Images and quantifications of the proportion of Tbx18-YFP+ (green) cells that were **(A, B)** Sox2+ (red) and **(C)** the proportion of Sox2+/YFP+ cells with nuclearized Sox2 at 3, 7, and 14 days post-stroke. Arrows denote co-labelled cells. Scale bars = 50 µm. Data analyzed by one way ANOVA ($F_{2,9} = 0.7934$, $p = 0.4816$ for Sox2, $F_{2,9} = 3.434$, $p = 0.0779$ for nuclearized Sox2) (n=3-6 animals per time point).

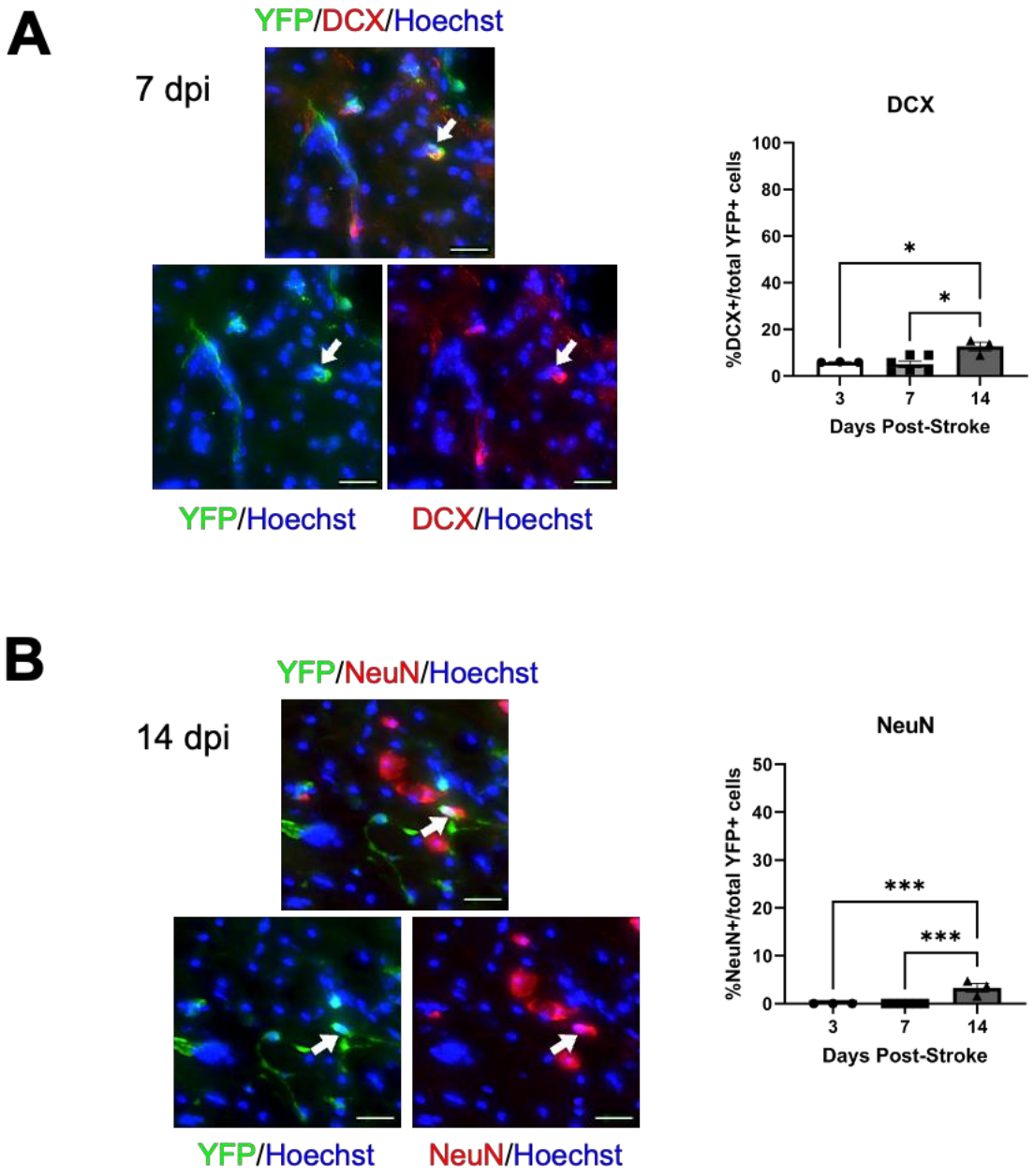

Figure 3: Ischemia-activated pericytes give rise to newborn neurons in the stroke lesion over time. (A-B) Images and quantifications of the proportion of Tbx18-YFP+ (green) cells that were **(A)** DCX+ and **(B)** NeuN+ (red) at 3, 7, and 14 days post-stroke. Arrows denote co-labelled cells. Scale bars = 20 μm. Data analyzed by one way ANOVA ($F_{2,9} = 7.075$, $p = 0.0142$ for DCX, $F_{2,9} = 22.01$, $p = 0.0003$ for NeuN) with Tukey's post-hoc test between time points (n=3-6 animals per time point, * $p < 0.05$, *** $p < 0.001$).

4.2 Compound C improves the efficiency of neural reprogramming of ischemia-activated pericytes

To evaluate the effect of compound C on pericyte reprogramming during the acute phase of stroke, Tbx18-YFP mice were treated with saline or compound C (10 mg/kg) daily for 5 days starting 24 hours following ET-1/L-NAME injections (Figure 4A). These mice were sacrificed at 7 days post-stroke to profile cell phenotypes. To determine whether compound C can facilitate the reprogramming of a-pericytes to i-NPCs, the proportion of Sox2+/YFP+ cells with nuclearized Sox2 in the stroke lesion was compared between treatment groups. At 7 days post-stroke in the compound C-treated animals, 16.97% of Sox2+/YFP+ cells had nuclearized Sox2 compared to only 4.48% in saline-treated animals (n=3, 6 respectively, p=0.003) (Figure 4B, C). There was no difference in the proportion of Tbx18-YFP+ cells expressing total Sox2 regardless of its signals in the nucleus or cytoplasm between groups (Figure 4D). The proportions of Tbx18-YFP+ cells expressing DCX (Figure 4E), adjacent to CD31+ blood vessels (Figure 4F), or expressing COL1A1 (Figure 4G) or Iba1 (Figure 4H) all remained similar between the compound C and vehicle treatment groups, indicating that compound C specifically enhanced the reprogramming efficiency of ischemia-activated pericytes into i-NPCs by facilitating Sox2 protein translocation from cytoplasm to nucleus.

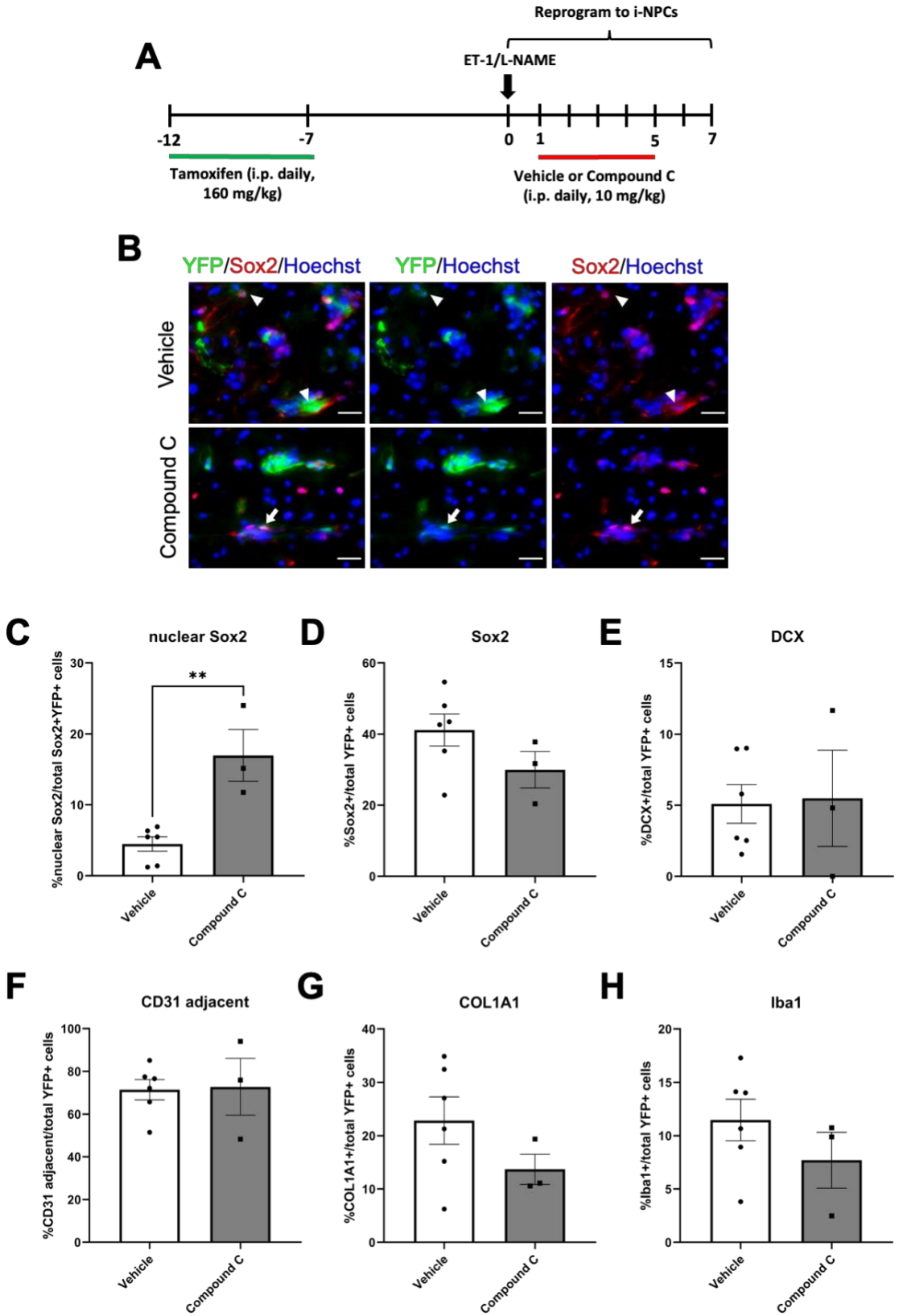
A
Reprogram to i-NPCs
ET-1/L-NAME
-12
-7
0
1
5
7
Tamoxifen (i.p. daily, 160 mg/kg)
Vehicle or Compound C (i.p. daily, 10 mg/kg)
B
YFP/Sox2/Hoechst
YFP/Hoechst
Sox2/Hoechst
Vehicle
Compound C
C
nuclear Sox2
%nuclear Sox2/total Sox2+YFP+ cells
**
D
Sox2
%Sox2+/total YFP+ cells
E
DCX
%DCX+/total YFP+ cells
F
CD31 adjacent
%CD31 adjacent/total YFP+ cells
G
COL1A1
%COL1A1+/total YFP+ cells
H
Iba1
%Iba1+/total YFP+ cells

Figure 4: Compound C enhances reprogramming efficiency of ischemia-activated pericytes. (A) Experimental timeline of TAM pre-treatment, ET-1/L-NAME surgery, and compound C administration schedule. **(B)** Images of Tbx18-YFP+ cell expressing Sox2. Arrows denote co-labelled cells with nuclearized Sox2, and arrowheads denote co-labelled cells with Sox2 mostly expressed in the cytoplasm. Scale bars = 20 μm. **(C)** Quantification of the proportion of Sox2+YFP+ cells with nuclearized Sox2 at 7 days post-stroke following vehicle or compound C treatment. **(D-H)** Quantifications of the proportion of Tbx18-YFP+ cells that were **(D)** Sox2+, **(E)** DCX+, **(F)** CD31 adjacent, **(G)** COL1A1+, and **(H)** Iba1+ at 7 days post-stroke following vehicle or compound C treatment. Data analyzed by Student's t-test (n=6 animals for vehicle, n=3 animals for compound C, ** $p < 0.01$).

4.3 Treatment with compound C followed by JZL184 does not increase neuron generation from ischemia-activated pericytes

Due to the relatively high mortality rate of mice during treatment with 160 mg/kg tamoxifen daily for 5 days (high dose tamoxifen) (Figure 5A), the dosage and treatment duration of tamoxifen was decreased to 120 mg/kg for 4 days (low dose tamoxifen) to maintain a sufficient number of animals to perform long-term post-stroke motor function recovery tests between treatment groups in each experimental cohort. The low dose tamoxifen treatment yielded minimal mortality amongst the treated animals. However, the total number of Tbx18-YFP+ cells per section was decreased at each time point as expected due to the decrease in tamoxifen to initiate recombination for YFP expression in Tbx18+ cells (Figure 5B, C).

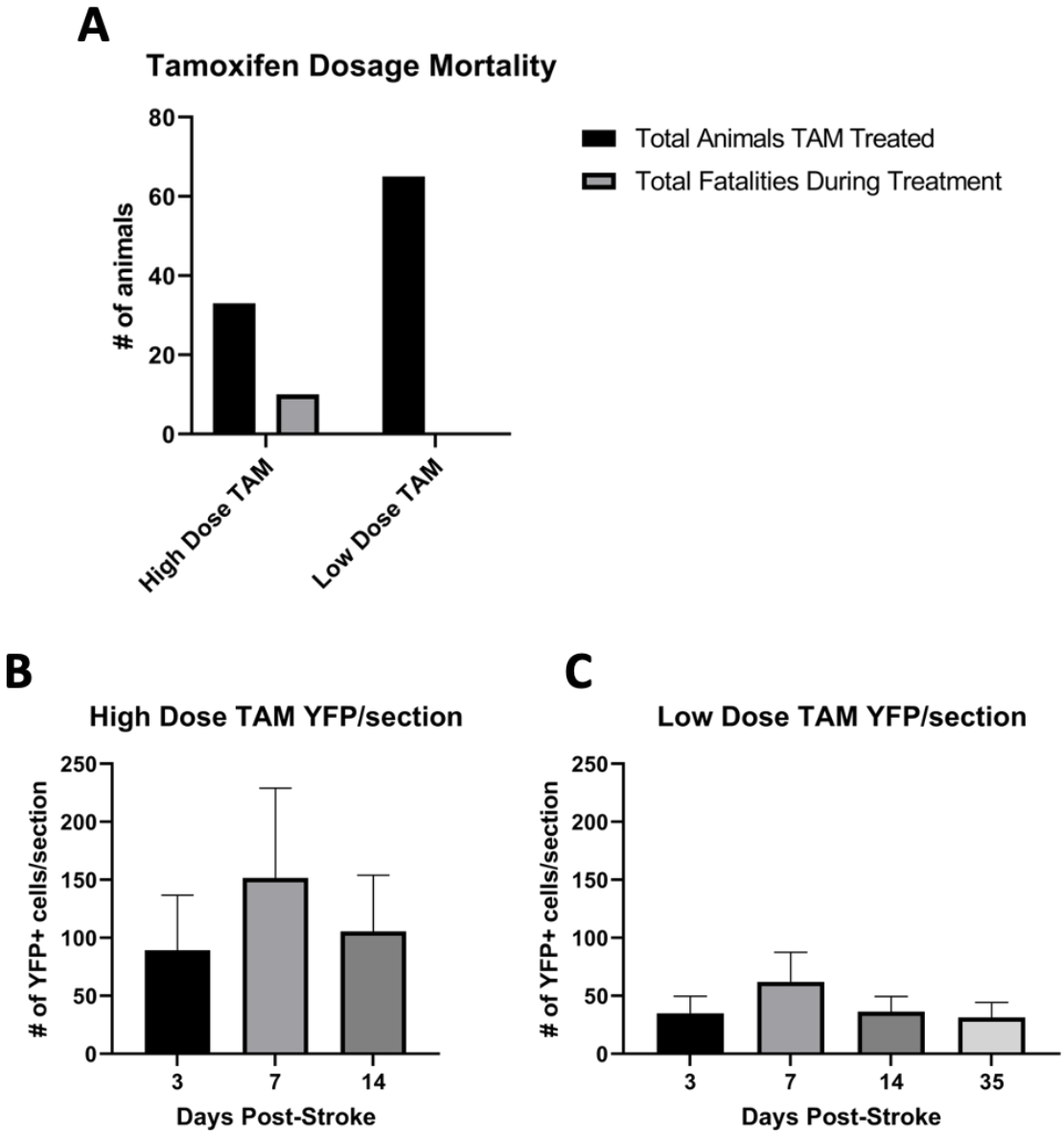

Figure 5: Lower tamoxifen dosage decreases mortality during treatment and recombination rate in Tbx18+ cells. (A) Comparison of animal mortality during treatment with high and low dose TAM. Quantifications of the average number of YFP+ cells per section across time points under **(B)** high dose (n=3 animals per time point) and **(C)** low dose (n=4-13 animals per time point) TAM treatments.

To determine whether acute treatment of compound C followed by chronic treatment of JZL184 post-stroke can facilitate the genesis of newborn neurons from a-pericytes, I used low dose tamoxifen (120mg/kg daily for 4 days) before stroke to lineage trace pericytes over 35 days post-stroke since the high mortality rate following high dose tamoxifen treatment was not suitable for long term tracing experiments. Mice were treated with compound C or vehicle as done previously. Compound C-treated mice were then administered with JZL184 every two days for the next four weeks (Figure 6A). Mice treated with vehicle in the acute phase (the first 7 days after stroke) continued with vehicle treatment for four weeks. By 14 days post-stroke, the combination drug-treated group showed a trend towards an increase in the proportion of DCX+ cells generated from Tbx18-YFP+ cells relative to the vehicle-treated group (10.52% versus 5.88%, n=9, 11 respectively, p=0.0905) (Figure 6C). All other cell types were found in similar proportions in vehicle- and combination drug-treated animals (Figure 6D-I).

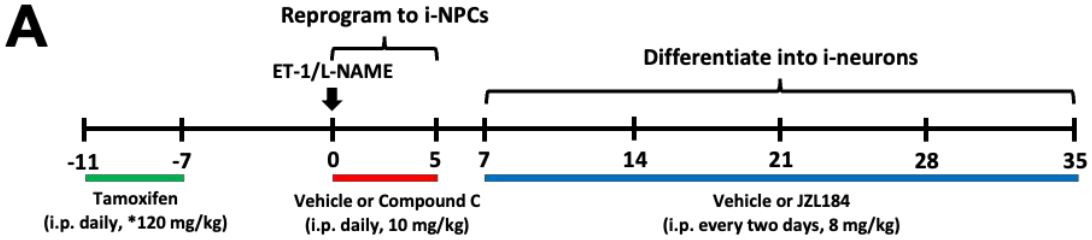

14 dpi
Vehicle vs Compound C + JZL

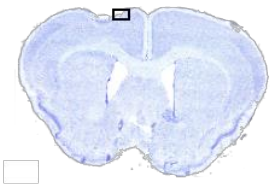

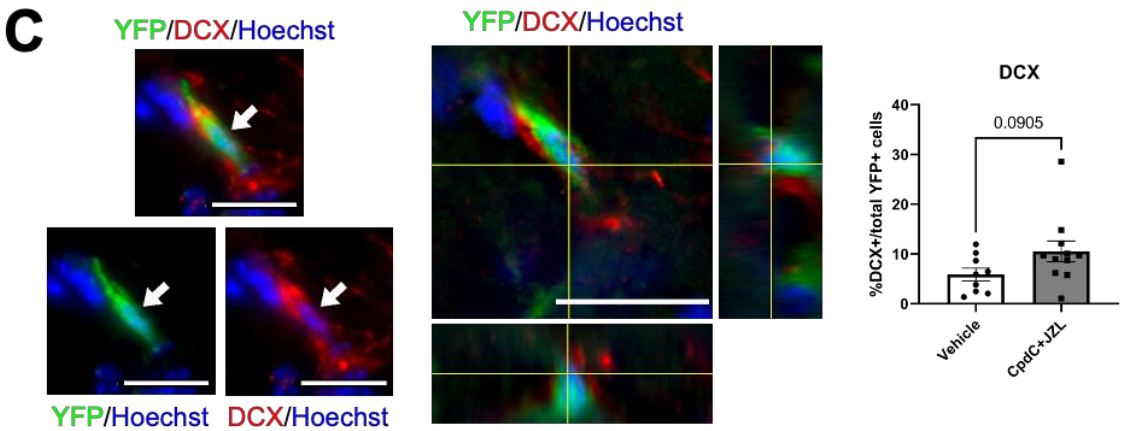

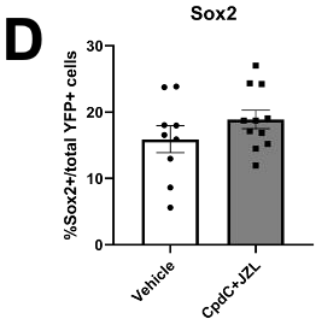

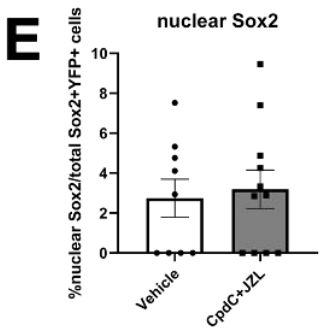

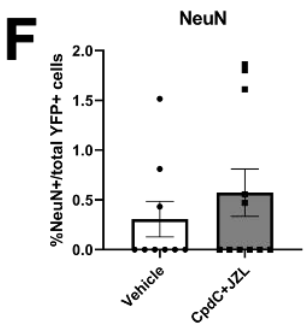

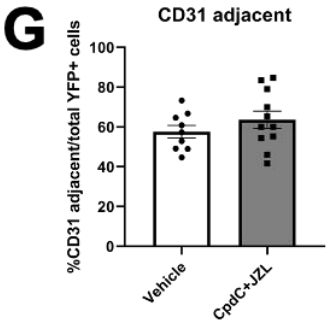

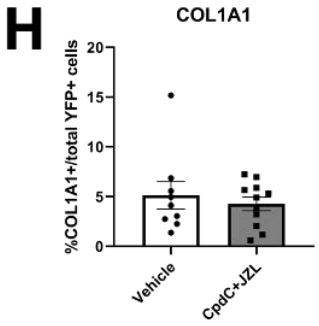

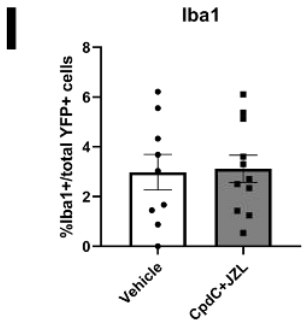

Figure 6: Compound C+JZL184 treatment has a minimal effect on increasing neurogenesis from Tbx18-YFP+ pericytes at 14 days post-stroke. (A) Experimental timeline of low dose TAM pre-treatment, ET-1/L-NAME surgery, and drug administration schedule. **(B)** Cresyl violet staining image of a representative area for identification of cells in the stroke lesion at 14 days post-stroke. **(C)** Quantification of the proportion of DCX+ (red) out of total Tbx18-YFP+ (green) cells and orthogonal image of a co-labelled DCX+/YFP+ cell at 14 days post-stroke. Scale bars = 20 μm in (C). **(D-I)** Quantifications of the proportion of Tbx18-YFP+ cells that were **(D)** Sox2+, **(E)** nuclearized Sox2 in total Sox2+/YFP+, **(F)** NeuN+, **(G)** CD31 adjacent, **(H)** COL1A1+, and **(I)** Iba1+ in vehicle or compound C+JZL184-treated mice 14 days post-stroke. Data analyzed by Student's t-test (n=9 animals for vehicle, n=11 animals for CpdC+JZL).

By 35 days following stroke, the proportion of NeuN+ neurons derived from Tbx18-YFP+ pericytes was similar between the two treatment groups (0.54% in vehicle-treated group, 0.81% in drug-treated group, n=13, 12 respectively, p=0.56) (Figure 7B). In addition, the proportions of CD31 adjacent, COL1A1+ fibroblasts, and Iba1+ microglia were comparable between groups as well (Figure 7C-E). Therefore, although some early effects of JZL184 on boosting neuronal differentiation in ischemia-activated pericytes had been found, there were no consistently increased neuron populations generated from Tbx18-YFP+ pericytes at the lesion site during the chronic phase following stroke.

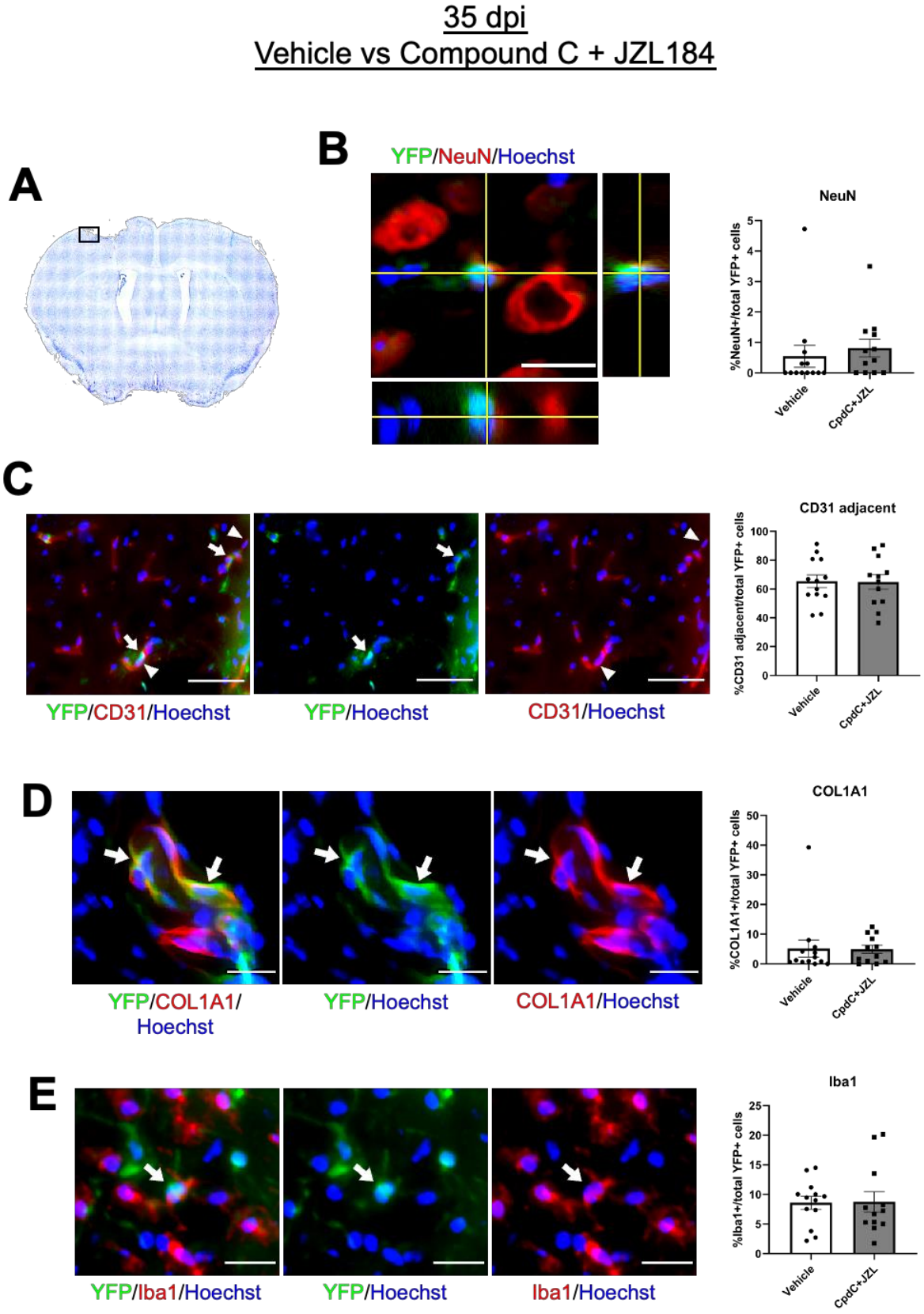
35 dpi
Vehicle vs Compound C + JZL184
A
B
YFP/NeuN/Hoechst
NeuN
%NeuN+/total YFP+ cells
Vehicle
CpdC+JZL
C
YFP/CD31/Hoechst
YFP/Hoechst
CD31/Hoechst
CD31 adjacent
%CD31 adjacent/total YFP+ cells
D
YFP/COL1A1/
Hoechst
YFP/Hoechst
COL1A1/Hoechst
COL1A1
%COL1A1+/total YFP+ cells
E
YFP/Iba1/Hoechst
YFP/Hoechst
Iba1/Hoechst
Iba1
%Iba1+/total YFP+ cells

Figure 7: Compound C+JZL184 treatment has no effect on Tbx18+ pericyte-derived mature neuron production at 35 days post-stroke. (A) Cresyl violet image of a representative area for identification of cells in the stroke lesion at 35 days post-stroke. **(B)** Quantification of the proportion of NeuN+ (red) cells out of total Tbx18-YFP+ (green) cells and orthogonal image of a co-labelled NeuN+/YFP+ cell at 35 days post-stroke. Quantifications of the proportion of Tbx18-YFP+ cells that were **(C)** CD31 adjacent, **(D)** COL1A1+, and **(E)** Iba1+ in vehicle or compound C+JZL184-treated mice 35 days post-stroke. Arrows denote co-labelled cells, arrowheads in (C) denote adjacent CD31+ cells. Scale bars = 20 μm in (B), (D), and (E), = 50 μm in (C). Data analyzed by Student's t-test (n=13 animals for vehicle, n=12 animals for CpdC+JZL).

4.4 Combination drug treatment does not affect stroke volume

To determine if the combination drug treatment had any effect on the extent of injury to the brain tissue, infarct volume was measured using cresyl violet staining. At 7 days post-stroke, there was no difference in stroke volume between vehicle and compound C+JZL184-treated groups (1.33 mm^3 in the vehicle treatment group, 1.18 mm^3 in the drug treatment group) (Figure 8A, B). Stroke volume was also comparable at 14 days (1.43 mm^3 for both groups) (Figure 8A, C) and 35 days (1.00 mm^3 in the vehicle-treated group, 0.92 mm^3 in the drug-treated group) (Figure 8A, D). Therefore, compound C+JZL184 treatment did not have any effect on stroke volume.

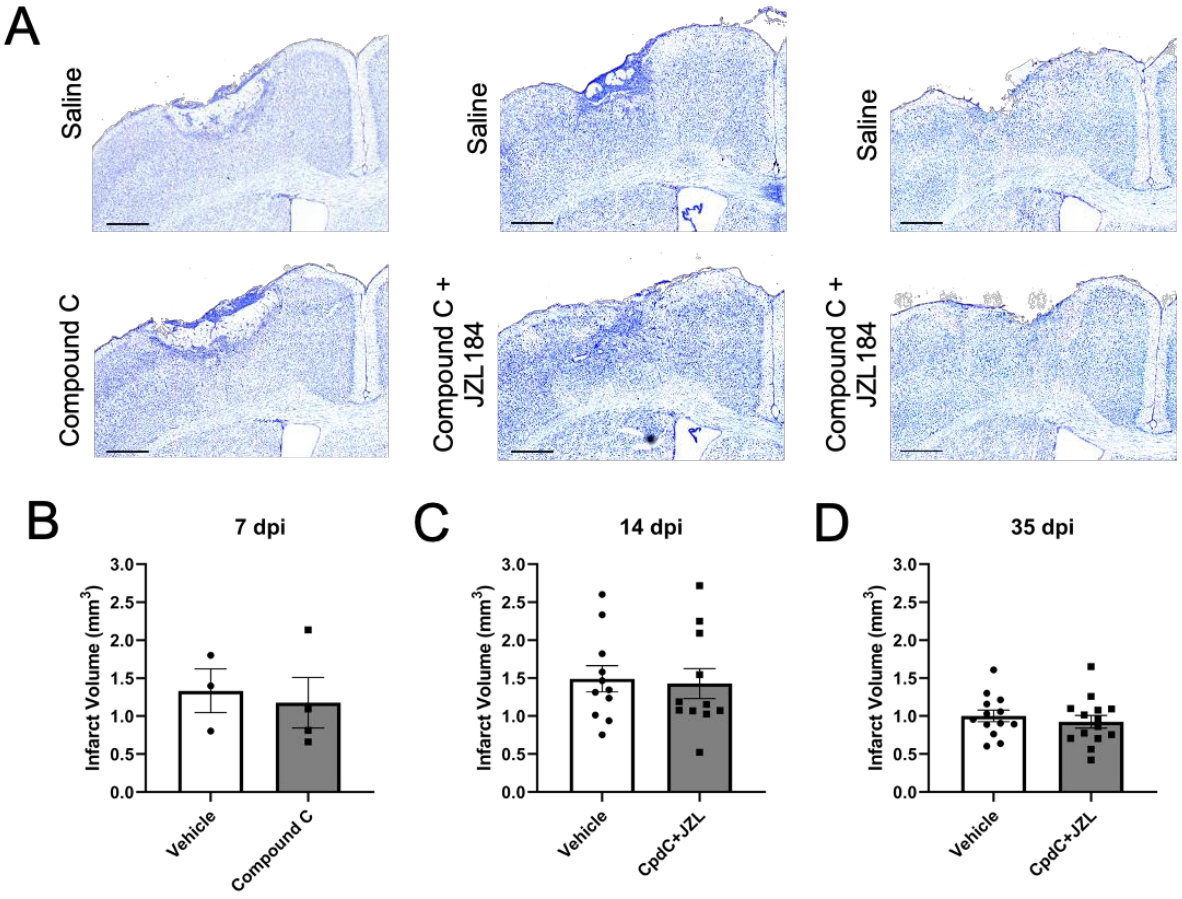

Figure 8: Compound C+JZL184 treatment has no effect on infarct volume. (A) Cresyl violet staining images and quantification of infarct volume at **(B)** 7, **(C)** 14, and **(D)** 35 days post-stroke with quantifications in vehicle versus drug-treated mice. Scale bars = 1 mm. Data analyzed with Student's t-test (n=3-4 animals per group at 7 days, n=11 animals per group at 14 days, n=13-14 animals per group at 35 days).

4.5 Combination drug treatment has a minimal effect on the pattern of post-stroke motor function recovery

Mice were tested on a battery of motor function tests, including the ladder rung test, cylinder test, and grid walk test, to compare post-stroke recovery between vehicle-treated and combination drug-treated animals. On the ladder rung test, coordinated sensorimotor function was assessed in the forelimbs and hindlimbs. Both groups showed a similar deficit in their contralateral forelimbs at 7 days after stroke, manifested by significantly increased percentages of error steps that the contralateral forelimbs took when compared to their respective pre-stroke baseline performance (Figure 9A). Compound C+JZL184 and vehicle treatment mice showed similar patterns of recovery relative to their own group pre-stroke baseline performance at all post-stroke time points. At 35 days post-stroke, both groups of mice can cross the ladder with minimal errors, similar to their pre-stroke baseline accuracy. No significant impairment to the ipsilateral forelimb (Figure 9B) or either side hindlimb (data not shown) was detected at any time point.

A

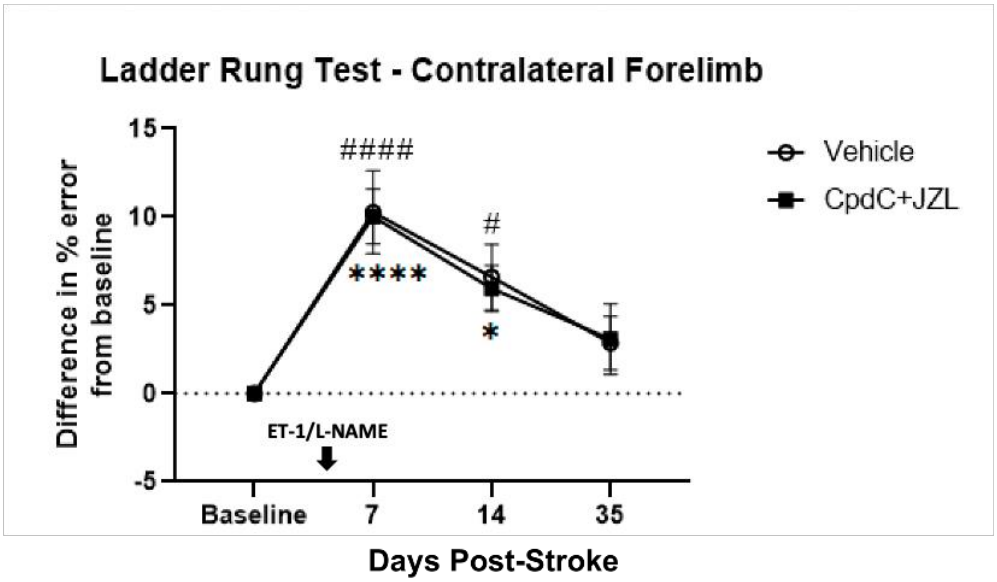
Ladder Rung Test - Contralateral Forelimb
Difference in % error from baseline
15
10
5
0
-5
####
#
****
*
ET-1/L-NAME
Baseline
7
14
35
Days Post-Stroke
Vehicle
CpdC+JZL

B

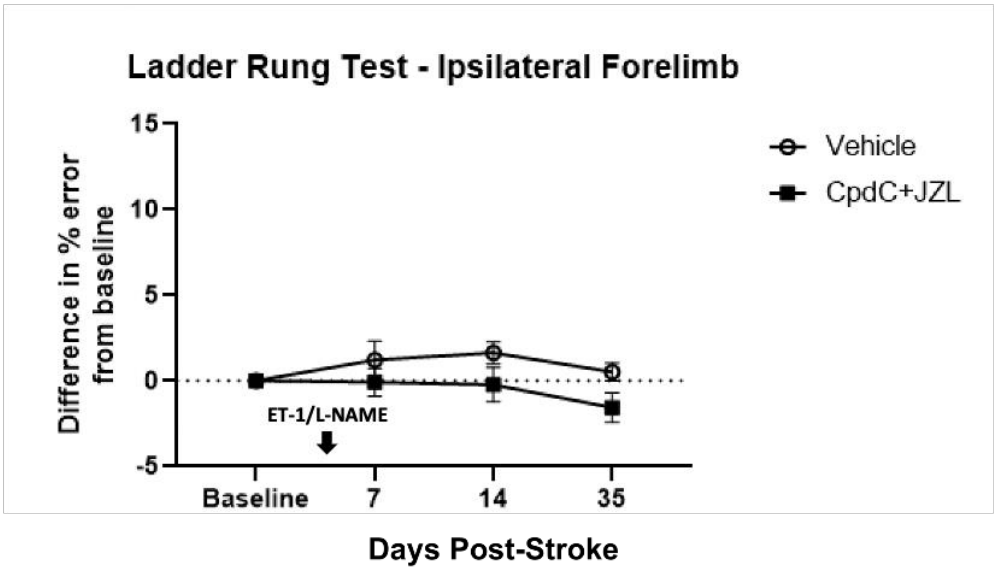
Ladder Rung Test - Ipsilateral Forelimb
Difference in % error from baseline
15
10
5
0
-5
ET-1/L-NAME
Baseline
7
14
35
Days Post-Stroke
Vehicle
CpdC+JZL

C

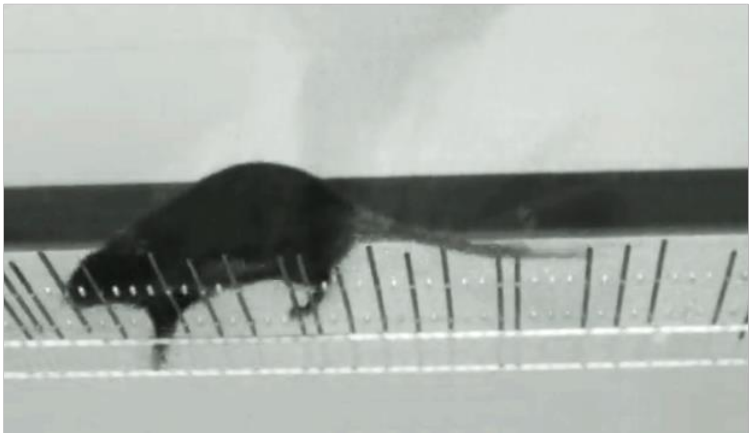

Figure 9: Compound C+JZL184 treatment does not affect ladder rung test performance. **(A)** Percentage of contralateral forelimb error steps relative to pre-stroke baseline (subtracting pre-stroke % error steps) on the ladder rung test at 7-, 14-, and 35-days post-stroke with vehicle or compound C+JZL184 treatment. Data was analyzed by two-way ANOVA (Treatment x Time Point $F_{(3,112)} = 0.02591$, $p = 0.9943$; Time Point $F_{(3,112)} = 18.46$, $p < 0.0001$; Treatment $F_{(1,112)} = 0.02039$, $p = 0.8852$, n = 8-19 animals for CpdC+JZL group, n = 7-16 animals for vehicle group) with Tukey's post-hoc test in comparison to their own pre-stroke baseline data (* $p < 0.05$, **** $p < 0.0001$ relative to CpdC+JZL baseline; # $p < 0.05$, #### $p < 0.0001$ relative to vehicle baseline). **(B)** Percentage of ipsilateral forelimb error steps relative to pre-stroke baseline (subtracting pre-stroke % error steps) on the ladder rung test at 7, 14, and 35 days post-stroke with vehicle or compound C+JZL184 treatment. Data was analyzed by two-way ANOVA (Treatment x Time Point $F_{(3,112)} = 0.7118$, $p = 0.5469$; Time Point $F_{(3,112)} = 0.7816$, $p = 0.5067$; Treatment $F_{(1,112)} = 4.954$, $p = 0.0280$, n = 8-19 animals for CpdC+JZL group, n = 7-16 animals for vehicle group) with Tukey's post-hoc test in comparison to own group baseline data. **(C)** Sample frame of ladder rung test performance video used for analysis.

The cylinder test is used as a measure of spontaneous forepaw motor function and locomotor asymmetry. At baseline, neither group displayed a particular preference for use of either the ipsilateral or contralateral forepaw. Both groups exhibited deficits at 7 days post-stroke, represented by an increase in preference for usage of their ipsilateral, uninjured forepaws relative to their respective pre-stroke baseline. The vehicle-treated group displayed a significant increase in the use of the ipsilateral forepaw at 7 and 14 days post-stroke while the compound C+JZL184-treated group only showed an increase in the use of the ipsilateral forepaw at 7 days post-stroke (Figure 10A). By 35 days following ischemia, neither group showed a significant ipsilateral preference compared to baseline.

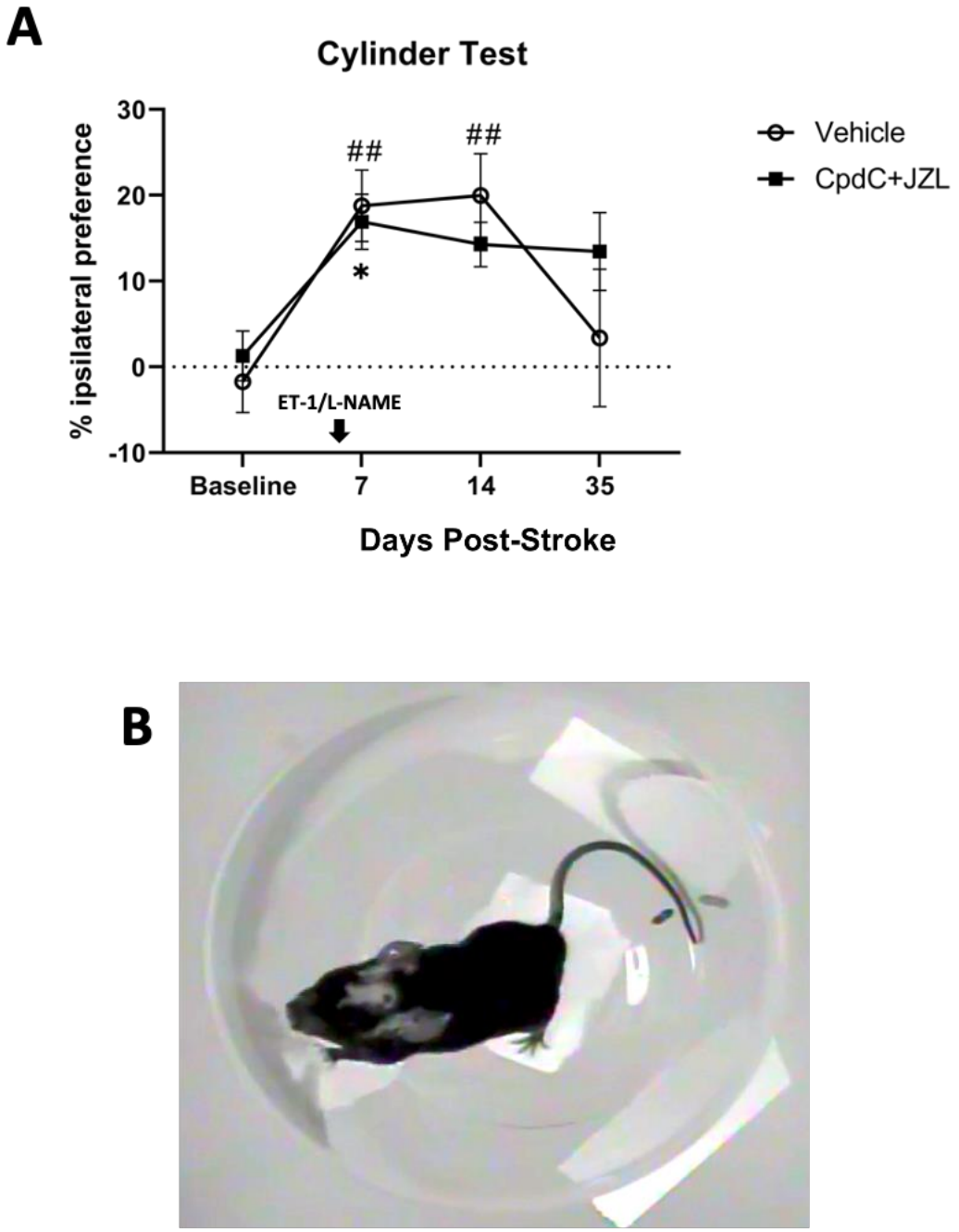

Figure 10: Compound C+JZL184 treatment modestly accelerates post-stroke forepaw recovery in the cylinder test. (A) Percentage ipsilateral preference on the cylinder test at baseline, 7-, 14-, and 35-days post-stroke with vehicle or compound C+JZL184 treatment. Data was analyzed by two-way ANOVA (Treatment x Time Point $F_{(3,112)} = 1.125$, $p = 0.3421$; Time Point $F_{(3,112)} = 10.84$, $p < 0.0001$; Treatment $F_{(1,112)} = 0.2155$, $p = 0.6434$, n = 8-19 animals for CpdC+JZL group, n = 7-16 animals for vehicle group) with Tukey's post-hoc test in comparison to their own pre-stroke baseline data (* $p < 0.05$, ## $p < 0.01$ relative to own pre-stroke baseline). **(B)** Sample frame of cylinder test performance video used for analysis.

The grid walk test assesses spontaneous motor coordination and sensorimotor function. Both vehicle and combination drug-treated groups showed a significant increase in the percentage of error in the contralateral forelimb at day 7 post-stroke relative to their respective pre-stroke baselines, with the vehicle-treated group exhibiting a less significant change relative to their baseline performance (Figure 11A). By 14 days post-stroke, both groups performed at a similar level compared to baseline. No significant difference in the number of error steps was observed in either group by day 35 post-stroke. No significant impairment to the ipsilateral forelimb (Figure 11B) was detected at any time point. Collectively, these behavioural results indicate that mice treated with compound C followed by JZL184 only had minimal changes to their pattern of recovery compared to vehicle-treated mice.

A

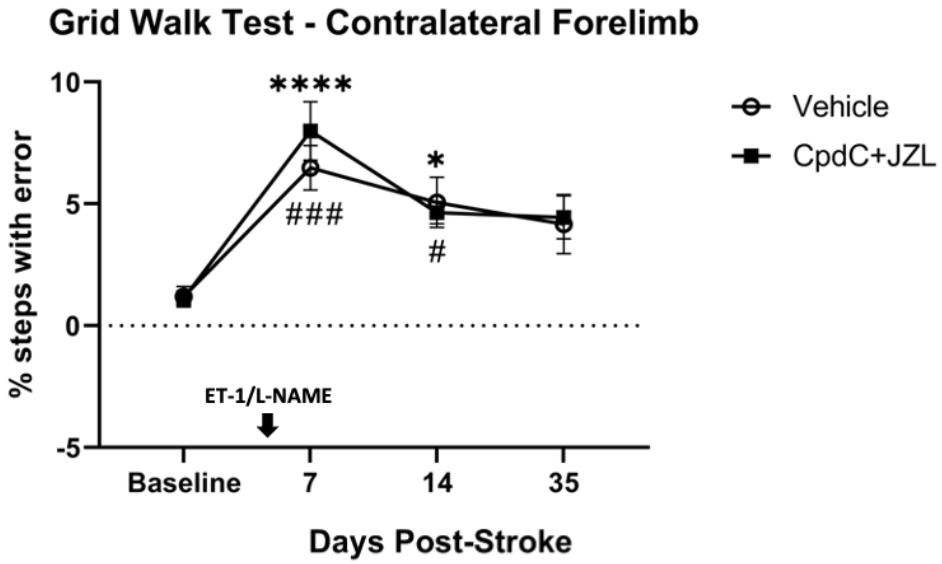
Grid Walk Test - Contralateral Forelimb
% steps with error
10
5
0
-5
****
###
*
#
ET-1/L-NAME
Baseline
7
14
35
Days Post-Stroke
Vehicle
CpdC+JZL

B

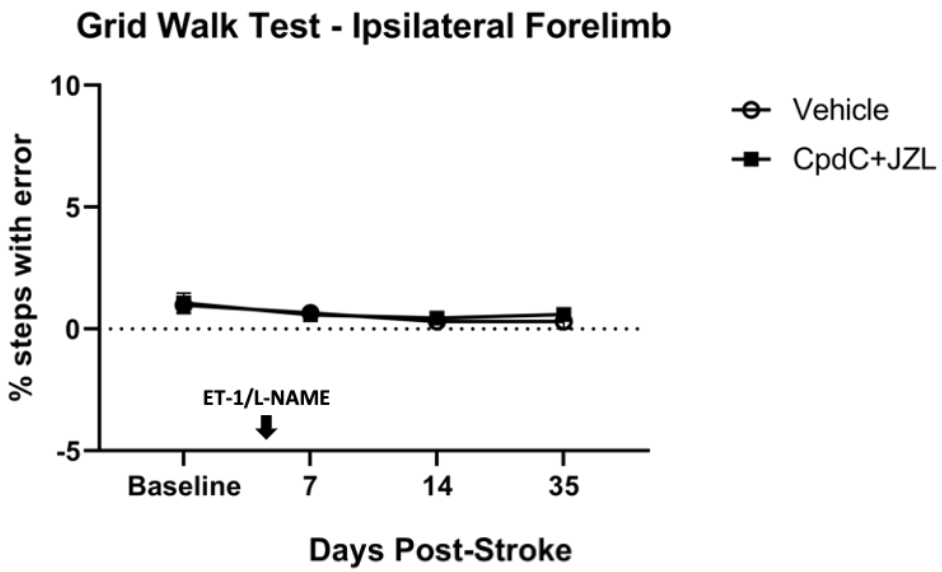
Grid Walk Test - Ipsilateral Forelimb
% steps with error
10
5
0
-5
ET-1/L-NAME
Baseline
7
14
35
Days Post-Stroke
Vehicle
CpdC+JZL

C

Figure 11: Compound C+JZL184 treatment has no effect on grid walk test performance. **(A)** Percentage of contralateral forelimb error steps on the grid walk test at 7-, 14-, and 35-days post-stroke with vehicle or compound C+JZL184 treatment. Data was analyzed by two-way ANOVA (Treatment x Time Point $F_{(3,112)} = 0.5733$, $p = 0.6338$; Time Point $F_{(3,112)} = 20.40$, $p < 0.0001$; Treatment $F_{(1,112)} = 0.2596$, $p = 0.6114$, n = 8-19 animals for CpdC+JZL group, n = 7-16 animals for vehicle group) with Tukey's post-hoc test in comparison to their own pre-stroke baseline (* $p < 0.05$, **** $p < 0.0001$ relative to CpdC+JZL baseline; # $p < 0.05$, ### $p < 0.001$ relative to vehicle baseline). **(B)** Percentage of ipsilateral forelimb error steps on the grid walk test at 7-, 14-, and 35-days post-stroke with vehicle or compound C+JZL184 treatment. Data was analyzed by two-way ANOVA (Treatment x Time Point $F_{(3,112)} = 0.1156$, $p = 0.9508$ Time Point $F_{(3,112)} = 2.445$, $p = 0.0677$; Treatment $F_{(1,112)} = 0.2712$, $p = 0.6035$, n = 8-19 animals for CpdC+JZL group, n = 7-16 animals for vehicle group) **(C)** Sample frame of grid walk test performance video used for analysis.

4.6 Tamoxifen treatment dosage affects the rate of reprogramming of ischemia-activated pericytes

To determine if decreasing the tamoxifen treatment dosage impacted reprogramming of a-pericytes, cellular analysis in the stroke lesion was performed using the new low dose tamoxifen treatment at the same time points as I did for high dose tamoxifen treatment. While the trends in the association of Tbx18-YFP+ cells with CD31+ blood vessels remained the same between low and high dose tamoxifen treatments (Figure 12A, B), all quantifications from other cell type markers following low dose tamoxifen treatment were different from those receiving high dose tamoxifen treatment. Across the 3, 7, and 14 day post-stroke time points, the proportions of both COL1A1+/YFP+ cells (6.98%, 6.28%, and 5.12% respectively) (Figure 12C, D) and Iba1+/YFP+ cells (5.54%, 4.19%, 2.98% respectively) (Figure 12E, F) were significantly smaller in the low dose tamoxifen group than in the high dose tamoxifen group.

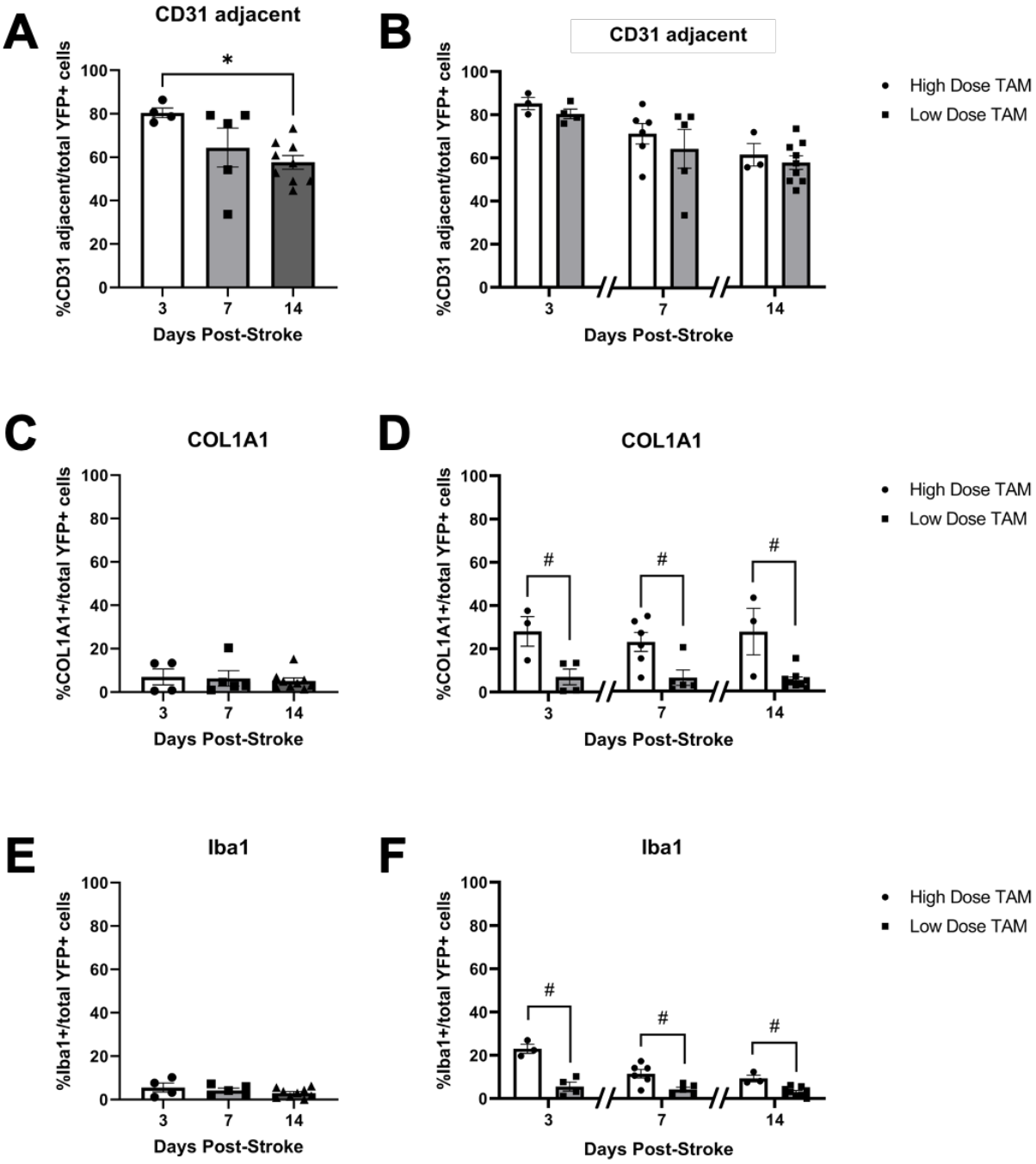

Figure 12: Low dose tamoxifen decreases reprogramming of pericytes to fibroblasts and microglia without altering vascular association. Quantifications of the proportion of Tbx18-YFP+ cells that were **(A)** CD31 adjacent, **(C)** COL1A1+, and **(E)** Iba1+ at 3, 7, and 14 days post-stroke in low dose TAM treated animals. Data analyzed by one way ANOVA ($F_{2,15}$ = 4.512, p = 0.0292 for CD31 adjacent; $F_{2,15}$ = 0.1472, p = 0.8644 for COL1A1; $F_{2,15}$ = 1.270, p = 0.3094 for Iba1) with Tukey's post-hoc test between time points (n=4, 5, 9 animals at 3, 7, 14 days post-stroke respectively, * $p < 0.05$). Comparison of quantifications of the proportion of Tbx18-YFP+ cells that were **(B)** CD31 adjacent, **(D)** COL1A1+, and **(F)** Iba1+ at 3, 7, and 14 days post-stroke with high dose or low dose TAM treatments. Data analyzed by Student's t-test (n=3-6 animals for high dose TAM, n=4-9 animals for low dose TAM, # $p < 0.05$).

In addition, the percentage of Sox2+/YFP+ cells gradually decreased over time after stroke in the low dose tamoxifen group (29.32% at 3 days, 14.22% at 7 days, 15.92% at 14 days) (Figure 13A). When compared to those in the high dose tamoxifen group, the proportions of Sox2+/YFP+ cells were decreased in the low dose tamoxifen group across all three time points (Figure 13B). However, the rate of Sox2 nuclearization in Sox2+/YFP+ cells was stable over time in the low dose tamoxifen group (6.53% at 3 days, 4.96% at 7 days, 2.74% at 14 days) (Figure 13C). Interestingly, a higher proportion of nuclearized Sox2 was found in the low TAM treatment group at 14 days post-stroke compared to the high dose TAM group (Figure 13D). The proportion of DCX+ neuroblasts over total Tbx18-YFP+ cells still increased significantly over time (from 0.62% at 3 days post-stroke to 5.88% at 14 days post-stroke) in the low dose tamoxifen group (Figure14A). However, DCX+ neuroblasts were found to make up a smaller proportion of Tbx18-YFP+ cells in the low dose tamoxifen group relative to the high dose tamoxifen group (Figure 14B). Finally, consistent with the initial results in the high dose tamoxifen group, no NeuN+/YFP+ cells were detected before day 14 in the low dose tamoxifen group (Figure 14C). However, the proportion of NeuN+ mature neurons produced from YFP+ cells was significantly reduced in the low dose tamoxifen group at day 14 post-stroke (0.31%) when compared to that in the high dose tamoxifen group (Figure 14D).

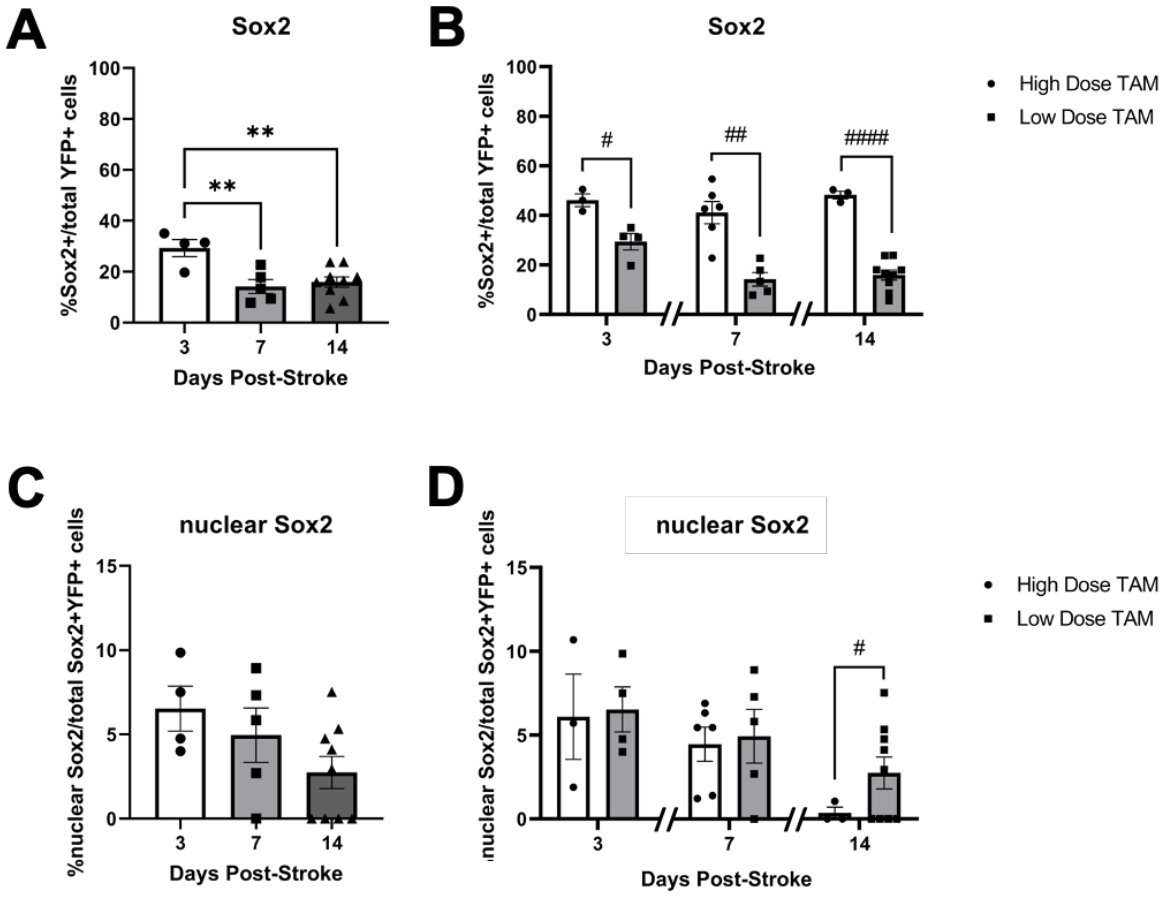

Figure 13: Low dose tamoxifen reduces the proportion of i-NPCs derived from Tbx18-YFP+ pericytes. **(A, C)** Quantification of **(A)** the proportion of Tbx18-YFP+ cells that were Sox2+ and **(C)** the proportion of Sox2+/YFP+ cells with nuclearized Sox2 at 3, 7, and 14 days post-stroke in low dose TAM treated animals. Data analyzed by one way ANOVA ($F_{2,15}$ = 7.923, p = 0.0045 for Sox2; $F_{2,15}$ = 2.362, p = 0.1283 for nuclear Sox2) with Tukey's post-hoc test between time points (n=4, 5, 9 animals at 3, 7, 14 days post-stroke respectively, ** $p < 0.01$). **(B, D)** Comparison of quantifications of **(B)** the proportion of Tbx18-YFP+ cells that were Sox2+ and **(D)** the proportion of Sox2+/YFP+ cells with nuclearized Sox2 at 3-, 7-, and 14-days post-stroke between high dose and low dose TAM treatment groups. Data analyzed by Student's t-test (n=3-6 animal per time point for high dose TAM, n=4-9 animals per time point for low dose TAM, # $p < 0.05$, ## $p < 0.01$, #### $p < 0.0001$).

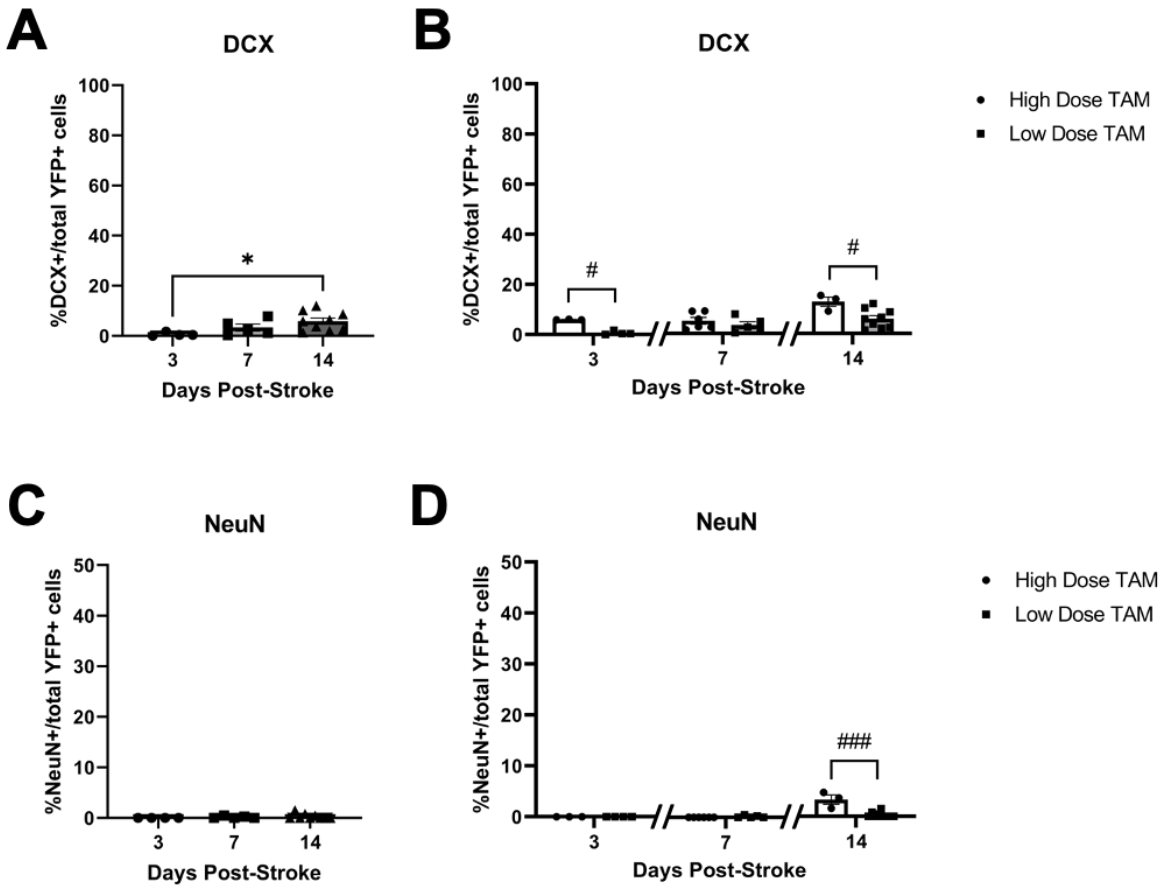

Figure 14: Low dose tamoxifen reduces the proportion of newborn and mature neurons derived from Tbx18-YFP+ pericytes. (A, C) Quantification of the proportion of Tbx18-YFP+ cells that were **(A)** DCX+ and **(C)** NeuN+ at 3, 7, and 14 days post-stroke in low dose TAM group. Data analyzed by one way ANOVA ($F_{2,15} = 3.892$, $p = 0.0435$ for DCX; $F_{2,15} = 0.8201$, $p = 0.4592$ for NeuN) with Tukey's post-hoc test between time points (n=4, 5, 9 animals at 3, 7, 14 days post-stroke respectively, * $p < 0.05$). **(B, D)** Comparison of quantifications of the proportion of Tbx18-YFP+ cells that were **(B)** DCX+ and **(D)** NeuN+ at 3, 7, and 14 days post-stroke between high dose and low dose TAM treatment groups. Data analyzed by Student's t-test (n=3-6 animals per time point for high dose TAM, n=4-9 animals per time point for low dose TAM, # $p < 0.05$, ### $p < 0.001$).

4.7 Tamoxifen treatment dosage interacts with compound C to influence ischemia-activated pericyte neural reprogramming

Given the differences found in reprogramming of a-pericytes between high and low dose tamoxifen treatments, I re-evaluated the effects of compound C on boosting a-pericyte to i-NPC reprogramming efficiency with low dose tamoxifen treatment. Compound C no longer produced a significant increase in Sox2 nuclearization when compared to the vehicle treatment group (7.46% of Sox2+/YFP+ cells in compound C-treated mice versus 4.96% of Sox2+/YFP+ cells in vehicle-treated mice, n=4-5 animals, p=0.8129) (Figure 15A). Low dose tamoxifen did not change the proportion of Sox2+, DCX+, CD31 adjacent, COLA1A1+, and Iba1+ cells over total YFP+ cells in the compound C-treated group (Figure 15B-F). Interestingly, the nuclearized Sox2+/YFP+ subpopulation was smaller in low dose tamoxifen groups receiving compound C treatment than that previously characterized in high dose tamoxifen group receiving compound C treatment (16.97% in high dose tamoxifen group versus 7.46% in low dose tamoxifen group all receiving compound C treatment, n=3-4 animals, p=0.0464) (Figure 15A). These findings suggest that high dose tamoxifen treatment prior to ischemic stroke may facilitate compound C's effect of enhancing reprogramming of a-pericyte into i-NPCs.

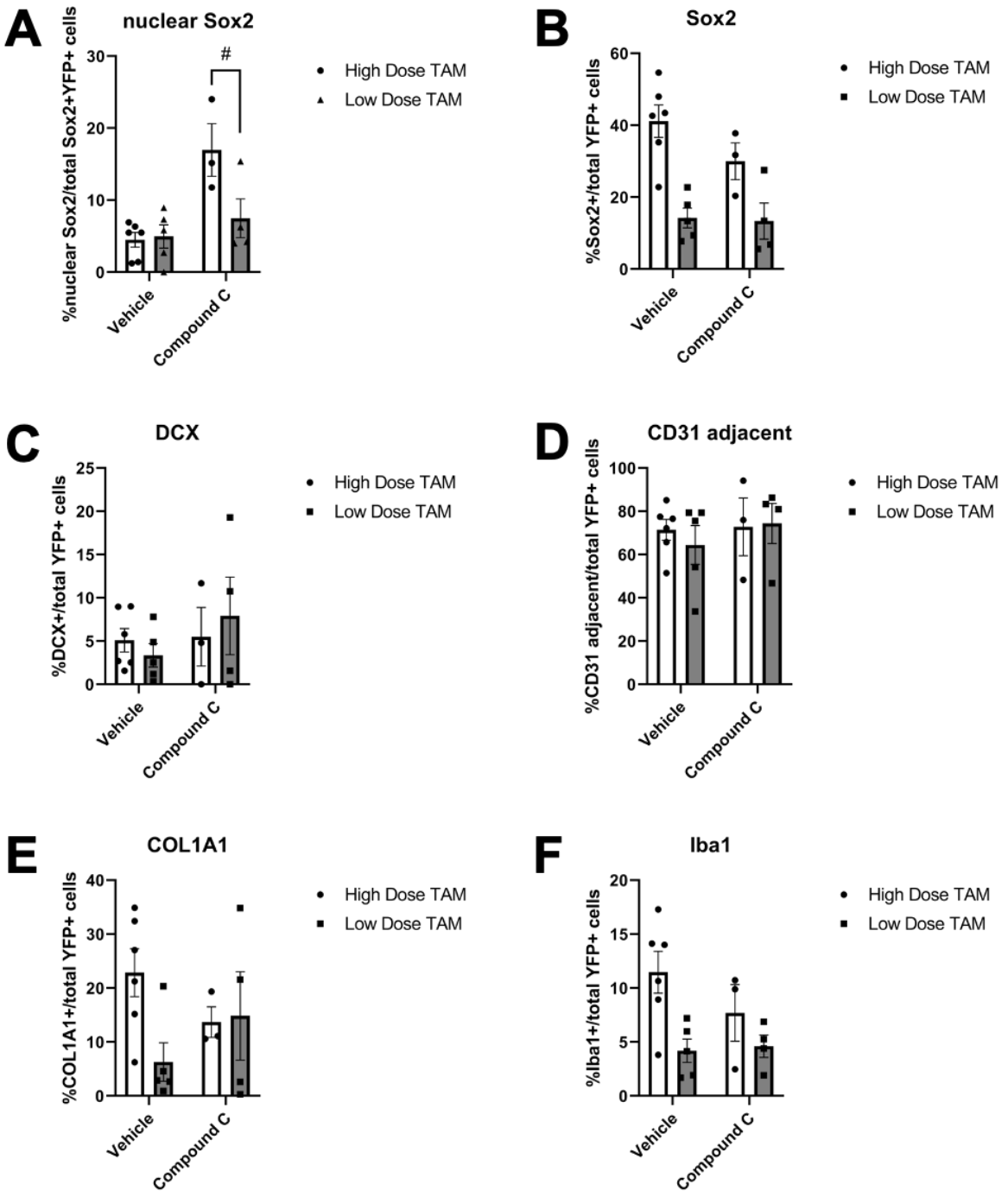

Figure 15: Tamoxifen interacts with compound C to influence reprogramming efficiency of ischemia-activated pericyte into i-NPCs. Comparison of **(A)** the proportion of Sox2+/YFP+ cells with nuclearized Sox2 and **(B-F)** the proportion of Tbx18-YFP+ cells that were **(B)** Sox2+, **(C)** DCX+, **(D)** CD31 adjacent, **(E)** COL1A1+, and **(F)** Iba1+ at 7 days post-stroke under high dose or low dose TAM treatment and vehicle or compound C treatment. Data analyzed by two-way ANOVA (Treatment x TAM Dosage $F_{(1,14)} = 5.885$, $p = 0.0294$; Treatment $F_{(1,14)} = 13.27$, $p = 0.0027$; TAM Dosage $F_{(1,14)} = 4.811$, $p = 0.0457$ for nuclear Sox2) followed by Tukey's post-hoc test (n=6 high dose TAM/vehicle, n=5 low dose TAM/vehicle, n=3 high dose TAM/compound C, n=4 low dose TAM/compound C, # $p < 0.05$).

5.0 Discussion

Using the ET-1/L-NAME focal cortical stroke model, together with the pericyte lineage tracing Tbx18-CreERT2/YFP-flx mouse line, I demonstrated that Tbx18+ pericytes can be reprogrammed into both neural and non-neural cell types in response to ischemic injury. In addition, pharmacological intervention with acute compound C treatment followed by chronic JZL184 treatment after stroke showed a trend to transiently enhance the newborn neuron population derived from Tbx18+ pericytes without altering the size of stroke volume and minimally affecting motor function recovery. Finally, I discovered that tamoxifen facilitates reprogramming of Tbx18+ pericytes in a dose-dependent manner.

5.1 Tbx18+ pericytes are reprogrammed into neural and non-neural cell types in response to ischemic injury

The present results uphold and build upon previous research reporting the existence of multipotent cells located adjacent to vascular endothelial cells and expressing pericyte markers exclusively in the ipsilateral lesion site in the brain.[65,76,78,102] Using the Tbx18-CreERT2/YFP-flx mouse line in the current study, I identified Tbx18-YFP+ pericytes as one group of cells from which these multipotent cells originate after stroke. This lineage tracing tool allowed me to examine pericyte reprogramming across multiple time points, from the acute phase (3 days after stroke) to chronic phase (35 days after stroke) following ischemic injury, whereas Nakagomi et al. (2011)'s early work focused on the acute phase (3 and 7 days post-stroke) following ischemic injury to identify locally induced-NPCs (i-NPCs) that are possibly derived from pericytes using immunohistochemical approaches. Intriguingly, both studies found that pericyte-derived i-NPCs were most abundant at day 3 post-stroke and decreased by day 7 post-stroke. In this regard, it will be important to sustain these i-NPC populations in the stroke lesion site to maximize the local neural regenerative potential, which was one of the aims of my

current study. My lineage tracing results also revealed that newborn immature and mature neurons can be generated from Tbx18-YFP+ pericytes at later time points (14 and 35 days post-stroke). This was supported by previous work showing that neurons can be produced from i-NPCs derived from ischemia-activated pericytes in culture.[78,102] Although the Tbx18+ pericyte-derived i-neurons following stroke are only generated sporadically, a potential pharmacological strategy that maximizes the genesis of these i-neurons will provide the regenerative potential to repair the stroke-damaged brain. In addition to neural cell types, I found that Tbx18+ a-pericytes can be reprogrammed into non-neural cell types, such as COL1A1+ fibroblasts and Iba1+ microglia. These findings were consistent with previous studies regarding the cellular plasticity of pericytes following ischemia, where these cells could express markers of fibroblasts[68,103] and microglia.[66,71] Although the role of these reprogrammed pericytes in fibrotic and inflammatory processes has not been explicitly studied yet, a more in-depth study of these reprogrammed cells would provide a holistic view of how ischemia-activated pericytes are involved in brain repair apart from their neurogenic potential.

The Tbx18-CreERT2 mouse line was created specifically for optimizing pericyte lineage tracing and was used to examine the plasticity of Tbx18+ brain pericytes following cortical stab injury.[50] Interestingly, Tbx18+ brain pericytes did not behave as multipotent stem cells to produce neural cells or produce collagen in response to a cortical stab injury.[50] However, in my study, Tbx18-YFP+ brain pericytes are capable of being reprogrammed into a variety of neural and non-neural cell phenotypes, including neural progenitors (Sox2+/YFP+) and fibroblasts (COL1A1+/YFP+) in response to ischemic stroke injury. This difference in response of Tbx18+ pericytes to physical injury (cortical stab injury) versus ischemic injury (vasoconstrictor action) as shown by these contrasting results reinforces the specific and unique ability of ischemia to naturally trigger brain pericyte plasticity *in situ*.

As pericytes are heterogeneous and can be identified by a variety of markers,[37] I had also examined ischemia-induced pericyte reprogramming using another pericyte lineage tracing mouse line, NG2-CreERT2/YFP-flx,[104–107] with the same approach. Approximately half of the NG2-YFP+ cells were closely associated with CD31+ blood vessels at 3 days post-stroke within the stroke lesion site, with only a small proportion of NG2-YFP+ cells co-expressing Tbx18 (Appendix Figure 16A, B). This suggests that Tbx18 and NG2 label distinct subpopulations of pericytes. Surprisingly, a high proportion of NG2-YFP+ cells expressed nuclearized Sox2, suggesting a stronger predisposition towards neural cell fate in reprogramming NG2-YFP+ cells than Tbx18+ pericytes (Appendix Figure 17A, B). Reprogrammed NG2-YFP+ NPCs expressed nuclearized Sox2 exclusively in the lesioned cortex and were not present in the uninjured contralateral cortex (Appendix Figure 17C). Additionally, NG2-YFP+ cells co-expressed COL1A1 and Iba1 (Appendix Figure 18A, B), arguing that different subpopulations of brain pericytes share the common characteristic of multipotency to produce neural and non-neural cell types in response to ischemic injury. However, one caveat of using NG2-YFP to trace pericytes is that NG2 is considered less specific to pericytes in the brain than Tbx18 since NG2 is also expressed in oligodendrocyte precursors. To reconcile the difference in specificity, future work with single-cell RNA sequencing analysis of NG2-YFP+ cells isolated from injured stroke tissues will be performed to examine specific cell trajectory changes.

5.2 Compound C+JZL184 combination drug treatment minimally enhances neurogenesis derived from Tbx18+ pericytes

In the current drug treatment paradigm, compound C, an inhibitor of AMPK, was used to enhance reprogramming of a-pericytes into i-NPCs immediately following stroke to expand the limited pool of i-NPCs. The subsequent treatment with JZL184, an inhibitor of Mgll, was

applied to further differentiate the i-NPCs into i-neurons. This paradigm has been successfully employed in an a-pericyte culture model by other lab members. However, in the current study, I only observed a trend towards higher DCX+/Tbx18-YFP+ immature neurons in the combination drug treatment group at 14 days post-stroke. This increase in DCX+/Tbx18-YFP+ immature neurons did not translate to increased numbers of NeuN+/Tbx18-YFP+ mature neurons at 35 days post-stroke in the combination drug treatment group. One earlier study has used a GFP lentivirus to trace i-NPCs at the ischemic lesion site in the MCAo stroke model and reported that none of the GFP labelled cells expressed neuronal markers by 21 days post-stroke.[75] My results similarly showed that Tbx18-YFP+ only sporadically expressed the mature neuron marker NeuN after 14 days post-stroke. These findings are in contrast with culture work showing that pericyte-derived i-NPCs *in vitro* can readily produce electrically active mature neurons.[102] Interestingly, Magnussen *et al.* (2020) performed an experiment comparing the neurogenic ability of endogenous adult NPCs when transplanted into either mouse striatum or cortex. The NPCs transplanted into the striatum generated more DCX+ neuroblasts and NeuN+ neurons than did the NPCs transplanted into the cortex.[108] Furthermore, they found that when both cortical astrocytes and striatal astrocytes are reprogrammed into i-NPCs via *Rbpj* gene deletion, i-NPCs derived from cortical astrocytes were less responsive to a locally injected EGF treatment to enhance neurogenesis than those derived from striatal astrocytes.[108] Along with the observation of a gradual decrease in the a-pericyte-derived i-NPC population within the ischemic lesion, lack of substantial neurogenesis in both vehicle and combination drug-treated mice *in vivo* may be due to the cortical location of ischemic tissue, which could present an innately unsupportive environment to neurogenesis.

Another possible factor in the lack of effectiveness of the combination drug treatments on local neural regeneration is that systemic administrations of drugs via intraperitoneal injection may dilute the drugs that would require a direct and fast delivery system for efficacy.

To address the issue, future work in the lab will focus on developing a novel and clinically applicable biomaterial that can be directly applied to the injured cortex to deliver targeted, sustained, and sequential release of compound C and JZL184. This new method would provide more confidence that the drugs will be delivered directly in a timely manner for the optimized duration of administration to maximize the local neural regenerative potential naturally triggered by ischemic insult.

I did not observe any consistent trends in patterns of recovery between the compound C+ZL184-treated groups and the vehicle-treated groups in the three motor behaviour tests. No difference between the groups was found on the ladder rung test and grid walk test. In contrast, drug treatment modestly accelerated motor functional recovery as measured on the cylinder test. The different results obtained from different tests could partially stem from the type of movement they assess. The ladder rung and grid walk tests involve all four limbs while the cylinder test primarily involves the forelimbs. The cylinder test may be more sensitive in these mice as ET-1/L-NAME stroke produced no persistent deficit in the hindlimbs as measured on the ladder rung test, which may have allowed for some compensatory function on tests involving all limbs.

5.3 Tamoxifen affects cellular reprogramming of ischemia-activated pericytes, interacting with compound C to regulate its efficacy

In the current study, I have employed two different dosages of tamoxifen for lineaging tracing. Interestingly, I discovered that tamoxifen impacts pericyte reprogramming in a dose-dependent manner, manifested by the low dose tamoxifen treatment group exhibiting decreased proportions of pericytes being reprogrammed into neural and non-neural cell types compared to the high dose tamoxifen group. One common feature between low dose and high dose tamoxifen was the proportion of vasculature (CD31)-associated Tbx18+ cells remaining

comparable at all time points with the same decreasing trend over time. Pericytes have been known to migrate away from vasculature in response to injury, remaining viable in the local parenchyma while non-migrating pericytes are more prone to exhibiting structural signs of degeneration.[109] This suggests that the decreasing proportions of vasculature-associated Tbx18+ cells may be indicative of the extent of tissue damage in the area caused by ischemic injury rather than a result of the pericytes losing their original function as part of the neurovascular unit to reprogram into other cell types.

In my study, the main role of tamoxifen within the inducible Cre-loxP genetic modification system is to bind to and facilitate the translocation of the estrogen receptor that is fused with Cre recombinase into the nucleus. Once inside the nucleus, the Cre recombinase removes the stop codon flanked by loxP sites to induce expression of fluorescent protein in cells expressing Tbx18. However, the differences found in a-pericyte reprogramming between high and low dosage tamoxifen treatments suggest that tamoxifen exposure beyond a certain dosage threshold may begin exerting a pronounced effect on cellular reprogramming, rather than solely carrying out its intended purpose of time-controlled fluorescent labelling. Specifically, high dose tamoxifen treatment boosts the effect of compound C on facilitating Sox2 nuclearization in Sox2+/Tbx18-YFP+ cells to complete i-NPC reprogramming from Tbx18+ pericytes. This phenotype was missing from low dose tamoxifen treatment.

Current research regarding the molecular activities of tamoxifen also provides clues for understanding the effect of tamoxifen on pericyte reprogramming. Indeed, it has been found that tamoxifen can directly affect multiple important proteins in the aPKC-CBP pathway. For example, tamoxifen increases AMPK activation via inhibition of mitochondrial complex I-mediated oxygen consumption, leading to an increased ratio of AMP/ATP.[110] It has been found that chronic pre-treatment with metformin, another AMPK activator, for 7 days can reduce AMPK activation caused by a subsequent permanent MCAO procedure, conferring protection

against ischemia-induced apoptosis.[111] It may be possible that the tamoxifen pre-treatment here acts in a similar manner as metformin administered before stroke, priming the aPKC-CBP pathway against stronger AMPK activation induced by the experimental ischemia. Post-stroke acute compound C treatment that further inhibits AMPK activation may produce stronger inhibition of the aPKC-CBP pathway, leading to an apparent boost in reprogramming efficiency in YFP labelled i-NPCs. Tamoxifen can also affect the aPKC-CBP pathway's downstream effects on neuronal differentiation mediated by endocannabinoid receptors whose signaling promotes neurogenesis,[88,112–114] including post-stroke neurogenesis.[115] Tamoxifen and its major active metabolites can bind to both CB1Rs and CB2Rs and act as inverse agonists.[116] Hence, in the period immediately following the ET-1/L-NAME procedure, tamoxifen compounds could have occupied these receptors and blocked neurogenesis. As a result, the increased i-NPC population under high dose tamoxifen treatment is attributable to enhanced facilitation of i-NPC reprogramming from a-pericytes.

Acquiring a greater understanding of tamoxifen's effect on cellular reprogramming would be a natural next step. Specifically, a culture model of hypoxia-induced pericyte reprogramming could be employed to examine the role of tamoxifen in pericyte reprogramming, mirroring the present *in vivo* experimental paradigm as closely as possible. Lastly, this should act as an important reminder regarding the precautions and considerations needed when examining neural cell processes under the Cre/loxP inducible system.

6.0 Conclusion

In summary, ischemia-activated Tbx18+ pericytes in the stroke lesion can be reprogrammed into neural cells, including NPCs, neuroblasts, and neurons, as well as non-neural cell types including fibroblasts and microglia. The combination drug treatment with compound C followed by JZL184 modestly alters the pattern of motor function recovery without great impact on local neurogenesis derived from ischemia-activated pericytes and stroke volumes over time. Significantly, I discovered that tamoxifen can affect pericyte reprogramming and interact with compound C to facilitate a boost in reprogramming efficiency. This study solidifies and advances existing knowledge of ischemia-activated pericyte reprogramming and differentiation and their potential in neural regenerative strategies. Some unexpected results also introduce a novel role of tamoxifen in cellular reprogramming, opening a new direction of study in the field.

References

1. Offner, H., Ihara, M., Schäbitz, W.-R. & Wong, P. T.-H. Stroke and other cerebrovascular diseases. *Neurochem Int* **107**, 1–3 (2017).

2. Chandra, A. *et al.* The cerebral circulation and cerebrovascular disease III: Stroke. in vol. 3 66–77 (2017).

3. Kaufmann, A. M. *et al.* Ischemic Core and Penumbra in Human Stroke. *Stroke* **30**, 93–99 (1999).

4. Feigin, V. L. *et al.* World Stroke Organization (WSO): Global Stroke Fact Sheet 2022. *Int J Stroke* **17**, 18–29 (2021).

5. NINDS. Post-Stroke Rehabilitation. https://www.stroke.nih.gov/documents/Post-Stroke_Rehabilitation_english_brochure_508C.pdf (2020).

6. Carmichael, S. T. Rodent models of focal stroke: Size, mechanism, and purpose. *Neurorx* **2**, 396–409 (2005).

7. Ng, Y. S., Stein, J., Ning, M. & Black-Schaffer, R. M. Comparison of Clinical Characteristics and Functional Outcomes of Ischemic Stroke in Different Vascular Territories. *Stroke* **38**, 2309–2314 (2007).

8. Fluri, F., Schuhmann, M. K. & Kleinschnitz, C. Animal models of ischemic stroke and their application in clinical research. *Drug Des Dev Ther* **9**, 3445–3454 (2015).

9. Corbett, D. & Thornhill, J. Temperature Modulation (Hypothermic and Hyperthermic Conditions) and Its Influence on Histological and Behavioral Outcomes Following Cerebral Ischemia. *Brain Pathol* **10**, 145–152 (2000).

10. Labat-gest, V. & Tomasi, S. Photothrombotic Ischemia: A Minimally Invasive and Reproducible Photochemical Cortical Lesion Model for Mouse Stroke Studies. *J Vis Exp* **e50370**, (2013).

11. Bruggen, N. van *et al.* T2- and diffusion-weighted magnetic resonance imaging of a focal ischemic lesion in rat brain. *Stroke* **23**, 576–582 (1992).

12. Lee, V. M. *et al.* Evolution of Photochemically Induced Focal Cerebral Ischemia in the Rat: Magnetic Resonance Imaging and Histology. *Stroke* **27**, 2110–2119 (1996).

13. Horie, N. *et al.* Mouse model of focal cerebral ischemia using endothelin-1. *J Neurosci Meth* **173**, 286–290 (2008).

14. Uchida, H. *et al.* Experimental model of small subcortical infarcts in mice with long-lasting functional disabilities. *Brain Res* **1629**, 318–328 (2015).

15. Roome, R. B. *et al.* A reproducible Endothelin-1 model of forelimb motor cortex stroke in the mouse. *J Neurosci Meth* **233**, 34–44 (2014).

16. Biernaskie, J., Corbett, D., Peeling, J., Wells, J. & Lei, H. A serial MR study of cerebral blood flow changes and lesion development following endothelin-1-induced ischemia in rats. *Magnet Reson Med* **46**, 827–830 (2001).

17. Uesugi, M., Kasuya, Y., Hayashi, K. & Goto, K. SB209670, a potent endothelin receptor antagonist, prevents or delays axonal degeneration after spinal cord injury. *Brain Res* **786**, 235–239 (1998).

18. Uesugi, M. *et al.* Endogenous endothelin-1 initiates astrocytic growth after spinal cord injury. *Brain Res* **728**, 255–259 (1996).

19. Carmichael, S. T. Cellular and molecular mechanisms of neural repair after stroke: Making waves. *Ann Neurol* **59**, 735–742 (2006).

20. Alia, C. *et al.* Neuroplastic Changes Following Brain Ischemia and their Contribution to Stroke Recovery: Novel Approaches in Neurorehabilitation. *Front Cell Neurosci* **11**, 76 (2017).

21. Ohab, J. J., Fleming, S., Blesch, A. & Carmichael, S. T. A Neurovascular Niche for Neurogenesis after Stroke. *J Neurosci* **26**, 13007–13016 (2006).

22. Lindvall, O. & Kokaia, Z. Neurogenesis following Stroke Affecting the Adult Brain. *Csh Perspect Biol* **7**, a019034 (2015).

23. Toman, N. G., Grande, A. W. & Low, W. C. Neural Repair in Stroke. *Cell Transplant* **28**, 1123–1126 (2019).

24. Takahashi, K. & Yamanaka, S. Induction of Pluripotent Stem Cells from Mouse Embryonic and Adult Fibroblast Cultures by Defined Factors. *Cell* **126**, 663–676 (2006).

25. Palma-Tortosa, S., Martin, B. C.-S., Kokaia, Z. & Tornero, D. Neuronal Replacement in Stem Cell Therapy for Stroke: Filling the Gap. *Frontiers Cell Dev Biology* **9**, 662636 (2021).

26. Mine, Y. *et al.* Grafted human neural stem cells enhance several steps of endogenous neurogenesis and improve behavioral recovery after middle cerebral artery occlusion in rats. *Neurobiol Dis* **52**, 191–203 (2013).

27. Chang, D.-J. *et al.* Therapeutic Potential of Human Induced Pluripotent Stem Cells in Experimental Stroke. *Cell Transplant* **22**, 1427–1440 (2012).

28. Niu, W. *et al.* In vivo reprogramming of astrocytes to neuroblasts in the adult brain. *Nat Cell Biol* **15**, 1164–1175 (2013).

29. Niu, W. *et al.* SOX2 Reprograms Resident Astrocytes into Neural Progenitors in the Adult Brain. *Stem Cell Rep* **4**, 780–794 (2015).

30. Zhang, L. *et al.* Reversing Glial Scar Back To Neural Tissue Through NeuroD1-Mediated Astrocyte-To-Neuron Conversion. *Biorxiv* 261438 (2018) doi:10.1101/261438.

31. Guo, Z. *et al.* In vivo direct reprogramming of reactive glial cells into functional neurons after brain injury and in an Alzheimer's disease model. *Cell Stem Cell* **14**, 188–202 (2013).

32. Chen, Y.-C. *et al.* A NeuroD1 AAV-Based Gene Therapy for Functional Brain Repair after Ischemic Injury through In Vivo Astrocyte-to-Neuron Conversion. *Mol Ther* **28**, 217–234 (2020).

33. Pereira, M. *et al.* Direct Reprogramming of Resident NG2 Glia into Neurons with Properties of Fast-Spiking Parvalbumin-Containing Interneurons. *Stem Cell Rep* **9**, 742–751 (2017).

34. Torper, O. *et al.* In Vivo Reprogramming of Striatal NG2 Glia into Functional Neurons that Integrate into Local Host Circuitry. *Cell Reports* **12**, 474–81 (2015).

35. Torper, O. *et al.* Generation of induced neurons via direct conversion in vivo. *Proc National Acad Sci* **110**, 7038–7043 (2013).

36. Mattugini, N. *et al.* Inducing Different Neuronal Subtypes from Astrocytes in the Injured Mouse Cerebral Cortex. *Neuron* **103**, 1086-1095.e5 (2019).

37. Yamazaki, T. & Mukouyama, Y. Tissue Specific Origin, Development, and Pathological Perspectives of Pericytes. *Frontiers Cardiovasc Medicine* **5**, 78 (2018).

38. Brown, L. S. *et al.* Pericytes and Neurovascular Function in the Healthy and Diseased Brain. *Front Cell Neurosci* **13**, 282 (2019).

39. Attwell, D., Mishra, A., Hall, C. N., O'Farrell, F. M. & Dalkara, T. What is a pericyte? *J Cereb Blood Flow Metabolism* **36**, 451–455 (2015).

40. Ozerdem, U., Grako, K. A., Dahlin-Huppe, K., Monosov, E. & Stallcup, W. B. NG2 proteoglycan is expressed exclusively by mural cells during vascular morphogenesis. *Dev Dynam* **222**, 218–227 (2001).

41. Stallcup, W. B. The NG2 proteoglycan: Past insights and future prospects. *J Neurocytol* **31**, 423 ppl= – 435 (2002).

42. Stallcup, W. B. The NG2 Proteoglycan in Pericyte Biology. *Adv Exp Med Biol* **1109**, 5–19 (2018).

43. Nehls, V. & Drenckhahn, D. Heterogeneity of microvascular pericytes for smooth muscle type alpha-actin. *J Cell Biology* **113**, 147–154 (1991).

44. Bandopadhyay, R. *et al.* Contractile proteins in pericytes at the blood-brain and blood-retinal barriers. *J Neurocytol* **30**, 35–44 (2001).

45. Nehls, V., Denzer, K. & Drenckhahn, D. Pericyte involvement in capillary sprouting during angiogenesis in situ. *Cell Tissue Res* **270**, 469–474 (1992).

46. Lindahl, P., Johansson, B. R., Levéen, P. & Betsholtz, C. Pericyte Loss and Microaneurysm Formation in PDGF-B-Deficient Mice. *Science* **277**, 242–245 (1997).

47. Winkler, E. A., Bell, R. D. & Zlokovic, B. V. Pericyte-specific expression of PDGF beta receptor in mouse models with normal and deficient PDGF beta receptor signaling. *Mol Neurodegener* **5**, 32 (2010).

48. Chen, J. *et al.* CD146 coordinates brain endothelial cell–pericyte communication for blood–brain barrier development. *Proc National Acad Sci* **114**, E7622–E7631 (2017).

49. Chen, J. *et al.* CD146 is essential for PDGFRβ-induced pericyte recruitment. *Protein Cell* **9**, 743–747 (2018).

50. Guimarães-Camboa, N. *et al.* Pericytes of Multiple Organs Do Not Behave as Mesenchymal Stem Cells In Vivo. *Cell Stem Cell* **20**, 345-359.e5 (2017).

51. McConnell, H. L., Kersch, C. N., Woltjer, R. L. & Neuwelt, E. A. The Translational Significance of the Neurovascular Unit*. *J Biol Chem* **292**, 762–770 (2017).

52. Kisler, K. *et al.* Pericyte degeneration leads to neurovascular uncoupling and limits oxygen supply to brain. *Nat Neurosci* **20**, 406–416 (2017).

53. Armulik, A. *et al.* Pericytes regulate the blood–brain barrier. *Nature* **468**, 557–561 (2010).

54. Villaseñor, R. *et al.* Region-specific permeability of the blood–brain barrier upon pericyte loss. *J Cereb Blood Flow Metabolism* **37**, 3683–3694 (2017).

55. Ma, Q. *et al.* Blood-brain barrier-associated pericytes internalize and clear aggregated amyloid-β42 by LRP1-dependent apolipoprotein E isoform-specific mechanism. *Mol Neurodegener* **13**, 57 (2018).

56. Sengillo, J. D. *et al.* Deficiency in Mural Vascular Cells Coincides with Blood–Brain Barrier Disruption in Alzheimer's Disease. *Brain Pathol* **23**, 303–310 (2013).

57. Jansson, D. *et al.* A role for human brain pericytes in neuroinflammation. *J Neuroinflamm* **11**, 104–104 (2014).

58. Rustenhoven, J., Jansson, D., Smyth, L. C. & Dragunow, M. Brain Pericytes As Mediators of Neuroinflammation. *Trends Pharmacol Sci* **38**, 291–304 (2017).

59. Meirelles, L. da S., Chagastelles, P. C. & Nardi, N. B. Mesenchymal stem cells reside in virtually all post-natal organs and tissues. *J Cell Sci* **119**, 2204–2213 (2006).

60. Beltrami, A. P. *et al.* Multipotent cells can be generated in vitro from several adult human organs (heart, liver, and bone marrow). *Blood* **110**, 3438–3446 (2007).

61. Feng, J., Mantesso, A. & Sharpe, P. T. Perivascular cells as mesenchymal stem cells. *Expert Opin Biol Th* **10**, 1441–1451 (2010).

62. Lv, F.-J., Tuan, R. S., Cheung, K. M. C. & Leung, V. Y. L. Concise Review: The Surface Markers and Identity of Human Mesenchymal Stem Cells. *Stem Cells* **32**, 1408–1419 (2014).

63. Zouani, O. F., Lei, Y. & Durrieu, M. Pericytes, Stem-Cell-Like Cells, but not Mesenchymal Stem Cells are Recruited to Support Microvascular Tube Stabilization. *Small* **9**, 3070–3075 (2013).

64. Blocki, A. *et al.* Not All MSCs Can Act as Pericytes: Functional In Vitro Assays to Distinguish Pericytes from Other Mesenchymal Stem Cells in Angiogenesis. *Stem Cells Dev* **22**, 2347–2355 (2013).

65. Tatebayashi, K. *et al.* Identification of Multipotent Stem Cells in Human Brain Tissue Following Stroke. *Stem Cells Dev* **26**, 787–797 (2017).

66. Sakuma, R. *et al.* Brain pericytes serve as microglia-generating multipotent vascular stem cells following ischemic stroke. *J Neuroinflamm* **13**, 57 (2016).

67. Oswald, J. *et al.* Mesenchymal Stem Cells Can Be Differentiated Into Endothelial Cells In Vitro. *Stem Cells* **22**, 377–384 (2004).

68. Birbrair, A. *et al.* Type-1 pericytes accumulate after tissue injury and produce collagen in an organ-dependent manner. *Stem Cell Res Ther* **5**, 122 (2014).

69. Göritz, C. *et al.* A Pericyte Origin of Spinal Cord Scar Tissue. *Science* **333**, 238–242 (2011).

70. Lee, C. H., Moioli, E. K. & Mao, J. J. Fibroblastic Differentiation of Human Mesenchymal Stem Cells using Connective Tissue Growth Factor. *2006 Int Conf Ieee Eng Medicine Biology Soc* 775–778 (2006) doi:10.1109/iembs.2006.259866.

71. Özen, I. *et al.* Brain pericytes acquire a microglial phenotype after stroke. *Acta Neuropathol* **128**, 381–396 (2014).

72. Rajbhandari, S. *et al.* Ischemia-Induced Multipotent Stem Cells Isolated from Stroke Patients Exhibit Higher Neurogenic Differentiation Potential than Bone Marrow-Derived Mesenchymal Stem Cells. *Stem Cells Dev* **29**, 994–1006 (2020).

73. Dore-Duffy, P., Katychev, A., Wang, X. & Buren, E. V. CNS Microvascular Pericytes Exhibit Multipotential Stem Cell Activity. *J Cereb Blood Flow Metabolism* **26**, 613–624 (2005).

74. Sakuma, R. *et al.* Comparative Characterization of Ischemia-Induced Brain Multipotent Stem Cells with Mesenchymal Stem Cells: Similarities and Differences. *Stem Cells Dev* **27**, 1322–1338 (2018).

75. Nakagomi, T. *et al.* Isolation and characterization of neural stem/progenitor cells from post-stroke cerebral cortex in mice. *Eur J Neurosci* **29**, 1842–1852 (2009).

76. Nakagomi, T. *et al.* Ischemia-Induced Neural Stem/Progenitor Cells in the Pia Mater Following Cortical Infarction. *Stem Cells Dev* **20**, 2037–2051 (2011).

77. Nakata, M. *et al.* Induction of Perivascular Neural Stem Cells and Possible Contribution to Neurogenesis Following Transient Brain Ischemia/Reperfusion Injury. *Transl Stroke Res* **8**, 131–143 (2017).

78. Gouveia, A. *et al.* The aPKC-CBP Pathway Regulates Post-stroke Neurovascular Remodeling and Functional Recovery. *Stem Cell Rep* **9**, 1735–1744 (2017).

79. Nakagomi, T. *et al.* Brain Vascular Pericytes Following Ischemia Have Multipotential Stem Cell Activity to Differentiate Into Neural and Vascular Lineage Cells. *Stem Cells* **33**, 1962–1974 (2015).

80. Schweizer, S., Meisel, A. & Märschenz, S. Epigenetic Mechanisms in Cerebral Ischemia. *J Cereb Blood Flow Metabolism* **33**, 1335–1346 (2013).

81. Hu, Z. *et al.* The Emerging Role of Epigenetics in Cerebral Ischemia. *Mol Neurobiol* **54**, 1887–1905 (2017).

82. Hamby, M. E., Coskun, V. & Sun, Y. E. Transcriptional regulation of neuronal differentiation: The epigenetic layer of complexity. *Biochimica Et Biophysica Acta Bba - Gene Regul Mech* **1779**, 432–437 (2008).

83. Basu, A. & Tiwari, V. K. Epigenetic reprogramming of cell identity: lessons from development for regenerative medicine. *Clin Epigenetics* **13**, 144 (2021).

84. Wang, J. *et al.* CBP Histone Acetyltransferase Activity Regulates Embryonic Neural Differentiation in the Normal and Rubinstein-Taybi Syndrome Brain. *Dev Cell* **18**, 114–125 (2010).

85. Wang, J. *et al.* Metformin Activates an Atypical PKC-CBP Pathway to Promote Neurogenesis and Enhance Spatial Memory Formation. *Cell Stem Cell* **11**, 23–35 (2012).

86. Dadwal, P. *et al.* Activating Endogenous Neural Precursor Cells Using Metformin Leads to Neural Repair and Functional Recovery in a Model of Childhood Brain Injury. *Stem Cell Rep* **5**, 166–173 (2015).

87. Gouveia, A. *et al.* The aPKC-CBP Pathway Regulates Adult Hippocampal Neurogenesis in an Age-Dependent Manner. *Stem Cell Rep* **7**, 719–734 (2016).

88. Syal, C. *et al.* Dysregulated expression of monoacylglycerol lipase is a marker for anti-diabetic drug metformin-targeted therapy to correct impaired neurogenesis and spatial memory in Alzheimer's disease. *Theranostics* **10**, 6337–6360 (2020).

89. Huang, Y. *et al.* An acetylation-enhanced interaction between transcription factor Sox2 and the steroid receptor coactivators facilitates Sox2 transcriptional activity and function. *J Biol Chem* **297**, 101389 (2021).

90. Baltus, G. A. *et al.* Acetylation of Sox2 Induces its Nuclear Export in Embryonic Stem Cells. *Stem Cells* **27**, 2175–2184 (2009).

91. Pevny, L. H. & Nicolis, S. K. Sox2 roles in neural stem cells. *Int J Biochem Cell Biology* **42**, 421–424 (2010).

92. Niu, W. *et al.* In vivo reprogramming of astrocytes to neuroblasts in the adult brain. *Nat Cell Biol* **15**, 1164–1175 (2013).

93. Ramamurthy, S. & Ronnett, G. V. Developing a head for energy sensing: AMP-activated protein kinase as a multifunctional metabolic sensor in the brain. *J Physiology* **574**, 85–93 (2006).

94. McCullough, L. D. *et al.* Pharmacological Inhibition of AMP-activated Protein Kinase Provides Neuroprotection in Stroke. *J Biol Chem* **280**, 20493–20502 (2005).

95. Li, J., Benashski, S. E., Siegel, C., Liu, F. & McCullough, L. D. Adenosine monophosphate activated protein kinase inhibition is protective in both sexes after experimental stroke. *Neurosci Lett* **482**, 62–65 (2010).

96. Khan, M., Dhammu, T. S., Matsuda, F., Singh, A. K. & Singh, I. Blocking a vicious cycle nNOS/peroxynitrite/AMPK by S-nitrosoglutathione: implication for stroke therapy. *Bmc Neurosci* **16**, 42 (2015).

97. Zanfirescu, A., Ungurianu, A., Mihai, D. P., Radulescu, D. & Nitulescu, G. M. Targeting Monoacylglycerol Lipase in Pursuit of Therapies for Neurological and Neurodegenerative Diseases. *Molecules* **26**, 5668 (2021).

98. Chanda, P. K. *et al.* Monoacylglycerol Lipase Activity Is a Critical Modulator of the Tone and Integrity of the Endocannabinoid System. *Mol Pharmacol* **78**, 996–1003 (2010).

99. Choi, S.-H. *et al.* Neuroprotective Effects of MAGL (Monoacylglycerol Lipase) Inhibitors in Experimental Ischemic Stroke. *Stroke* **49**, 718–726 (2018).

100. Nomura, D. K. *et al.* Endocannabinoid Hydrolysis Generates Brain Prostaglandins That Promote Neuroinflammation. *Science* **334**, 809–813 (2011).

101. Rahmani, M.-R., Shamsizadeh, A., Moghadam-Ahmadi, A., Kaeidi, A. & Allahtavakoli, M. Monoacylglycerol lipase inhibitor, JZL-184, confers neuroprotection in the mice middle cerebral artery occlusion model of stroke. *Life Sci* **198**, 143–148 (2018).

102. Nakagomi, T. *et al.* Brain Vascular Pericytes Following Ischemia Have Multipotential Stem Cell Activity to Differentiate Into Neural and Vascular Lineage Cells. *Stem Cells* **33**, 1962–1974 (2015).

103. Makihara, N. *et al.* Involvement of platelet-derived growth factor receptor β in fibrosis through extracellular matrix protein production after ischemic stroke. *Exp Neurol* **264**, 127–134 (2015).

104. Hosaka, K. *et al.* Pericyte–fibroblast transition promotes tumor growth and metastasis. *Proc National Acad Sci* **113**, E5618–E5627 (2016).

105. Mayr, D. *et al.* Characterization of the two inducible Cre recombinase-based mouse models NG2- CreER TM and PDGFRb-P2A-CreER T2 for pericyte labeling in the retina. *Curr Eye Res* (2021) doi:10.1080/02713683.2021.2002910.

106. Hartmann, D. A. *et al.* Pericyte structure and distribution in the cerebral cortex revealed by high-resolution imaging of transgenic mice. *Proc Spie* **2**, 041402–041402 (2015).

107. Berthiaume, A.-A. *et al.* Dynamic Remodeling of Pericytes In Vivo Maintains Capillary Coverage in the Adult Mouse Brain. *Cell Reports* **22**, 8–16 (2018).

108. Magnusson, J. P. *et al.* Activation of a neural stem cell transcriptional program in parenchymal astrocytes. *Elife* **9**, e59733 (2020).

109. Dore-Duffy, P. *et al.* Pericyte Migration from the Vascular Wall in Response to Traumatic Brain Injury. *Microvasc Res* **60**, 55–69 (2000).

110. Daurio, N. A. *et al.* AMPK Activation and Metabolic Reprogramming by Tamoxifen through Estrogen Receptor–Independent Mechanisms Suggests New Uses for This Therapeutic Modality in Cancer Treatment. *Cancer Res* **76**, 3295–3306 (2016).

111. Deng, T. *et al.* Pre-stroke Metformin Treatment is Neuroprotective Involving AMPK Reduction. *Neurochem Res* **41**, 2719–2727 (2016).

112. Diaz-Alonso, J. *et al.* The CB1 Cannabinoid Receptor Drives Corticospinal Motor Neuron Differentiation through the Ctip2/Satb2 Transcriptional Regulation Axis. *J Neurosci* **32**, 16651–16665 (2012).

113. Xapelli, S. *et al.* Activation of Type 1 Cannabinoid Receptor (CB1R) Promotes Neurogenesis in Murine Subventricular Zone Cell Cultures. *Plos One* **8**, e63529 (2013).

114. Jin, K. *et al.* Defective Adult Neurogenesis in CB1 Cannabinoid Receptor Knockout Mice. *Mol Pharmacol* **66**, 204–208 (2004).

115. Bravo-Ferrer, I. *et al.* Cannabinoid Type-2 Receptor Drives Neurogenesis and Improves Functional Outcome After Stroke. *Stroke* **48**, 204–212 (2017).

116. Ford, B. M., Franks, L. N., Radominska-Pandya, A. & Prather, P. L. Tamoxifen Isomers and Metabolites Exhibit Distinct Affinity and Activity at Cannabinoid Receptors: Potential Scaffold for Drug Development. *Plos One* **11**, e0167240 (2016).

Appendix

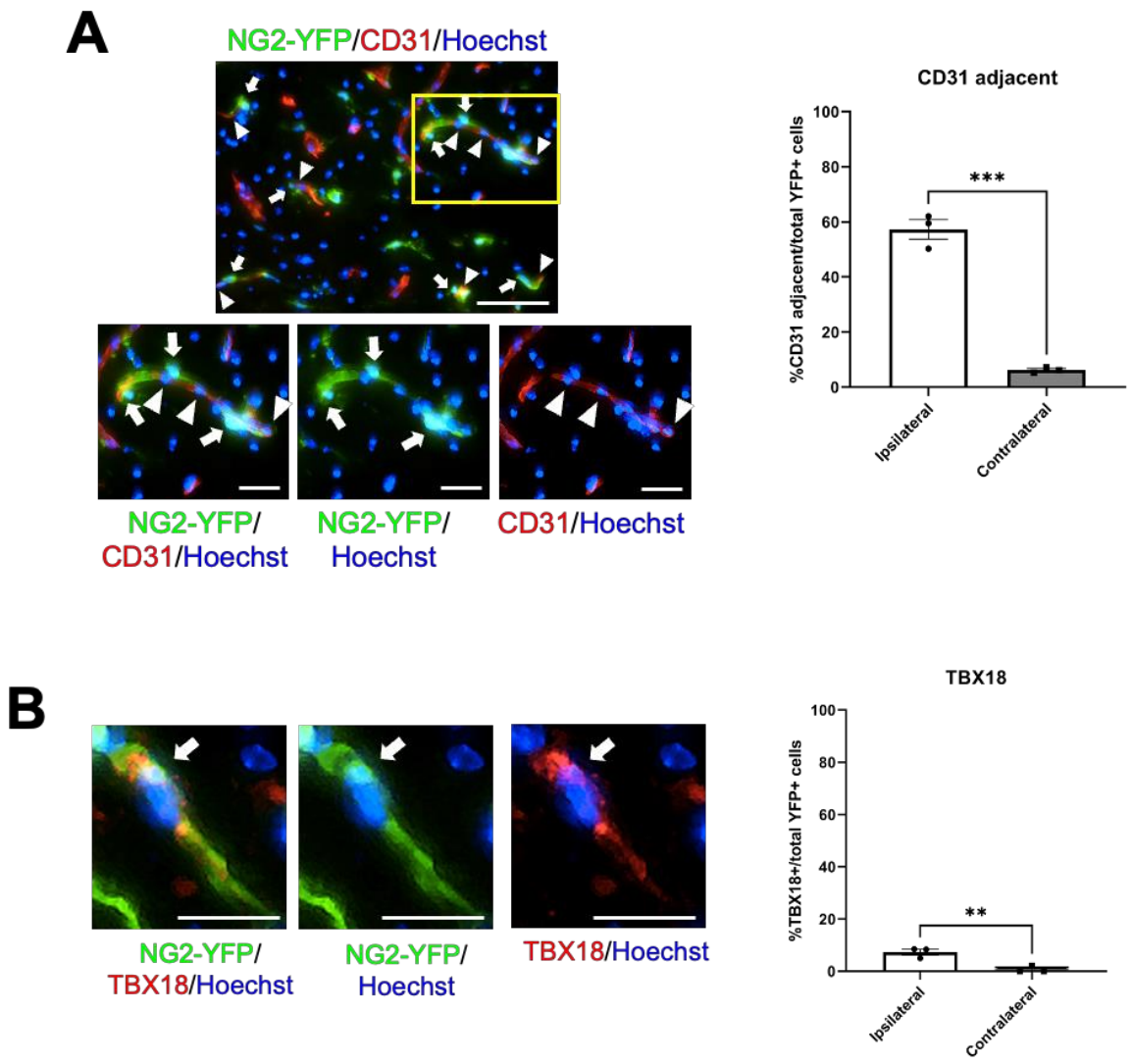

Appendix Figure 16: NG2+ ischemia-activated pericytes in the stroke lesion display reduced vascular association at 3 days post-stroke compared to Tbx18+ a-pericytes, represent distinct subpopulations of pericytes. Images and quantification of the proportion of NG2-YFP+ (green) cells that were **(A)** CD31 adjacent and **(B)** co-expressing TBX18 in the ipsilateral stroke lesion and contralateral cortex at 3 days post-stroke. Arrows denote co-labelled cells, arrowheads in (A) denote adjacent CD31+ cells. Scale bars = 50 μm in (A), 20 μm in (B). Data analyzed by Student's t-test (n=3 animals, ** $p < 0.01$, *** $p < 0.001$)

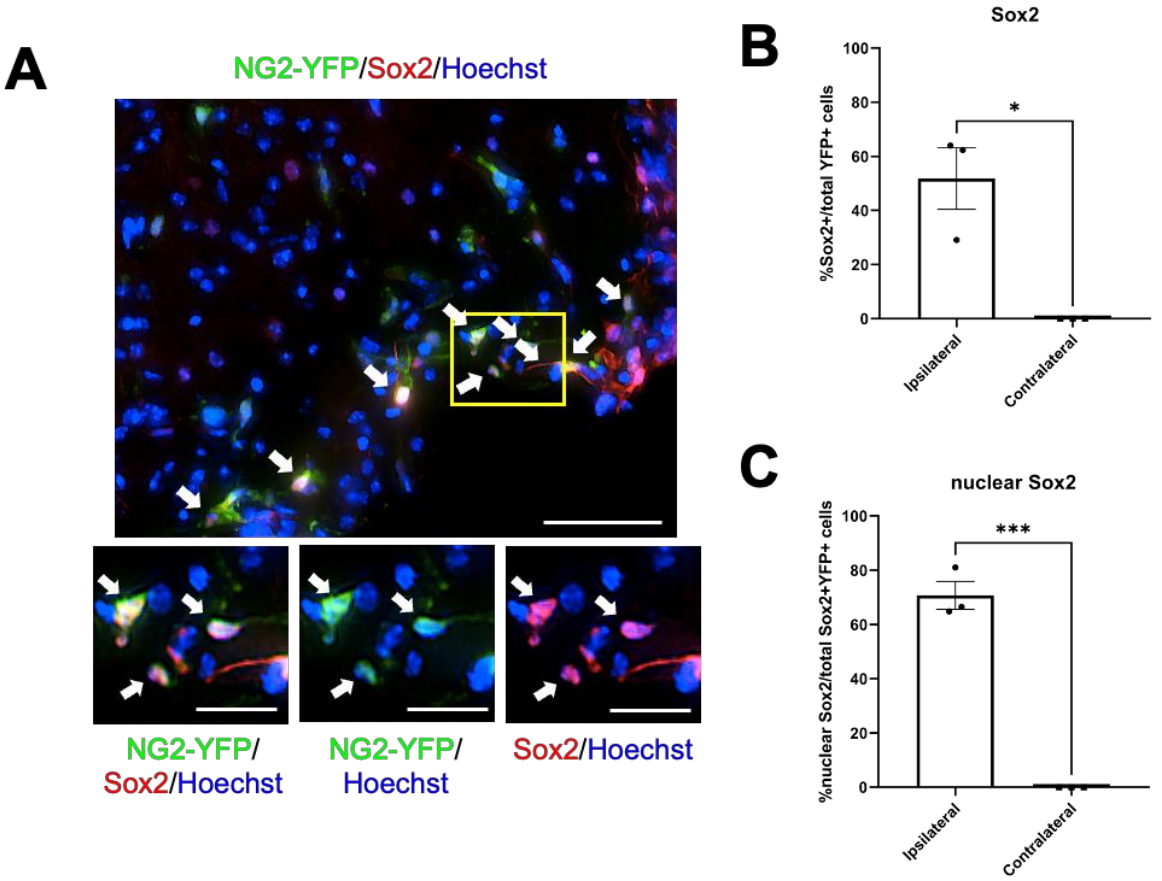

Appendix Figure 17: NG2+ ischemia-activated pericytes in the stroke lesion are reprogrammed into multipotent i-NPCs more readily than Tbx18+ a-pericytes. Images and quantification of the proportion of NG2-YFP+ (green) cells that were **(A, B)** Sox2 (red) and **(C)** the proportion of Sox2+/YFP+ cells with nuclearized Sox2 in the ipsilateral stroke lesion and contralateral cortex at 3 days post-stroke. Arrows denote co-labelled cells. Scale bars = 50 µm in upper overview image, 20 µm in lower close-up images. Data analyzed by Student's t-test (n=3 animals, * $p < 0.05$, *** $p < 0.001$)

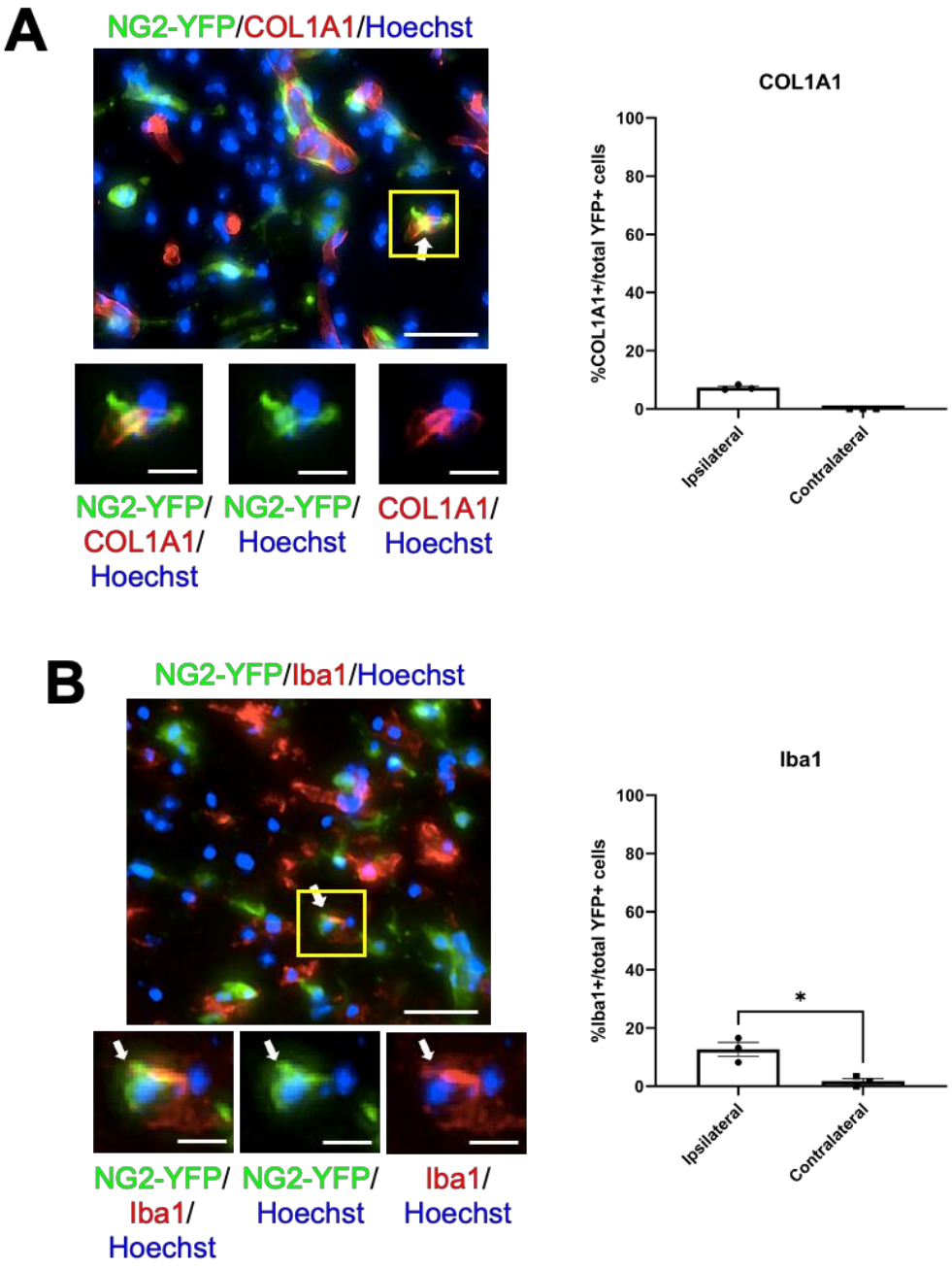

Appendix Figure 18: NG2+ ischemia-activated pericytes in the stroke lesion express non-neural cell type markers. Images and quantification of the proportion of NG2-YFP+ (green) cells that co-expressed **(A)** COL1A1 and **(B)** Iba1 in the ipsilateral stroke lesion and contralateral cortex at 3 days post-stroke. Arrows denote co-labelled cells. Scale bars = 20 μm in upper overview images, 10 μm in lower close-up images. Data analyzed by Student's t-test (n=3 animals, * $p < 0.05$)